8th BRNO EFEPR SCHOOL

Biological Applications of EPR

Marilena Di Valentin
Department of Chemical Sciences
University of Padova

Some figures are courtesy of Maxie Roessler, Pierre Dorlet, Enrica Bordignon, Alice Bowen and Wolfgang Lubitz

CEITEC

www.eprschool.ceitec.cz

EFEPR

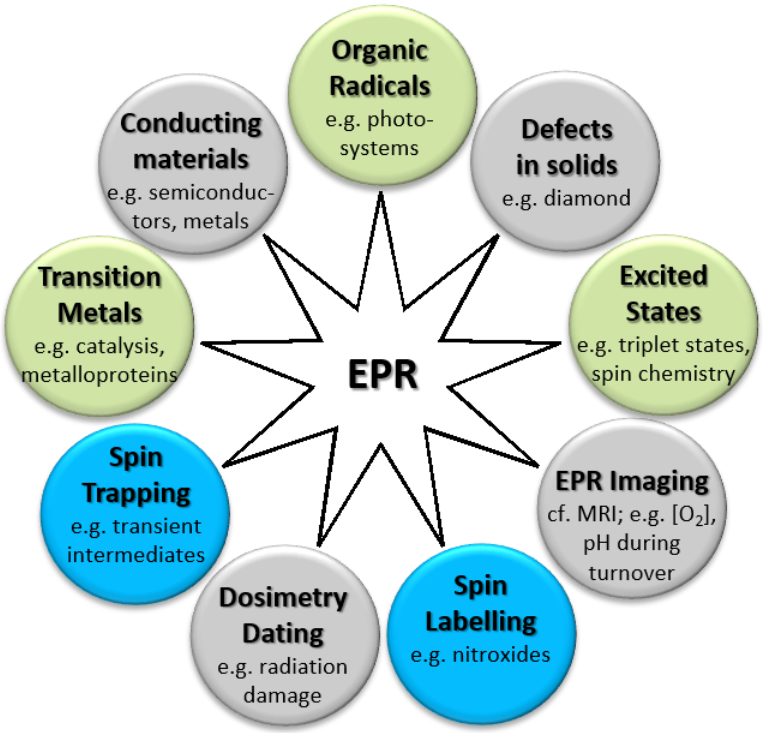

In biological systems we often rely on following ***intrinsic* paramagnetic centres**, such as:

- **Organic radicals** (semiquinones, chlorophylls, tyrosines)
- **Photoexcited states** (triplets, radical pairs)
- **Transition metals** (Cu^{2+}, Fe^{3+}, Mn^{2+}, Co^{2+})

We can often *introduce* paramagnetic centres, ***extrinsic* paramagnets**, or find ways to 'catch' short-lived intermediates:

- **Spin labels** (nitroxides, Gd^{3+})
- Spin trapping (e.g. superoxide)
- Rapid freeze quench

EPR has many 'non-bio' applications too …

The work flow in EPR:

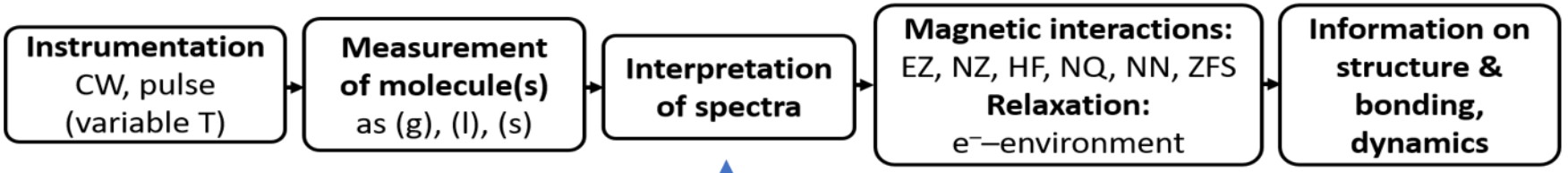

by simulations

by computation

The spin Hamiltonian:

$$\mathrm{H}_0 = \mathrm{H}_{\mathrm{EZ}} + \mathrm{H}_{\mathrm{NZ}} + \mathrm{H}_{\mathrm{HF}} + \mathrm{H}_{\mathrm{NQ}} + \mathrm{H}_{\mathrm{NN}} + \mathrm{H}_{\mathrm{ZFS}}$$

Spin Hamiltonian — Electron Zeeman — Nuclear Zeeman — Hyperfine — Nuclear quadrupole — Nuclear-nuclear — Zero-field splitting — interactions

$$H_0 = \mu_{\mathrm{B}}\mathbf{B}_0\mathbf{g}\mathbf{S}/\hbar - \beta_n \sum_{k=1}^{l} g_{n,k}\,\mathbf{B}_0\mathbf{I}_k/\hbar + \sum_{k=1}^{l} \mathbf{S}\mathbf{A}_k\mathbf{I}_k + \sum_{I_k>\frac{1}{2}} \mathbf{I}_k\mathbf{Q}_k\mathbf{I}_k + \sum_{i\neq k} \mathbf{I}_i\mathbf{d}_{ik}\mathbf{I}_k + \mathbf{SDS}$$

Pulse EPR enables to single out different interactions to gain a much more detailed understanding about a given spin system

High Field EPR enables resolve tensor components

Advanced EPR Techniques

Field-Swept Pulse EPR

High Frequency / High Field

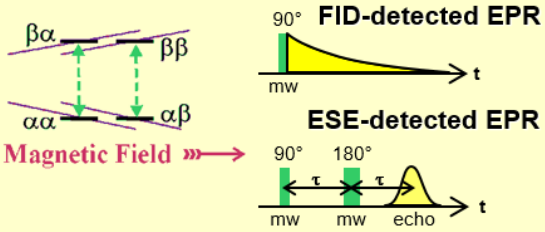

EPR spectra, ns time resolution

PELDOR-DEER

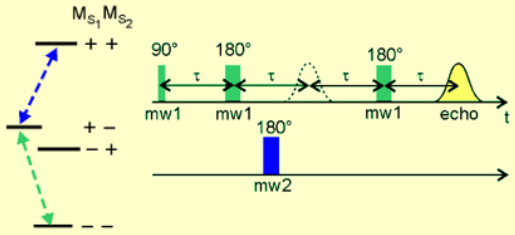

distance between electron spins

Echo Envelope Modulation

ESEEM

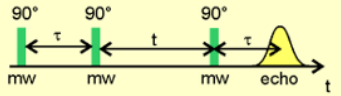

HYSCORE

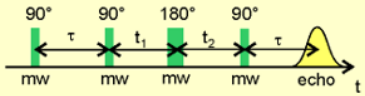

weakly coupled nuclei (hyperfine & quadrupole)

ELDOR-detected NMR

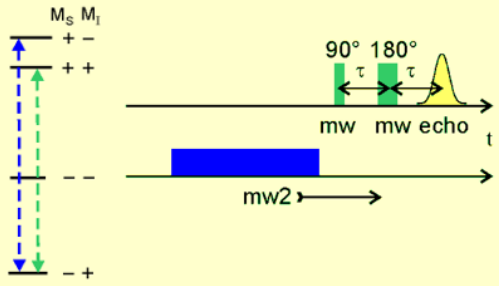

hfc of strongly coupled nuclei

Electron-Nuclear-Nuclear Triple Resonance

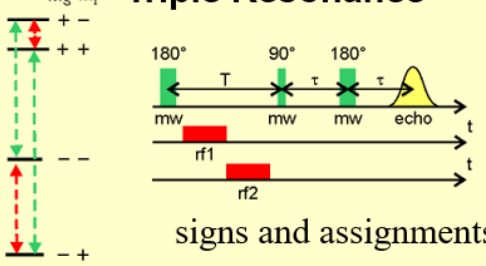

signs and assignments

Davies ENDOR

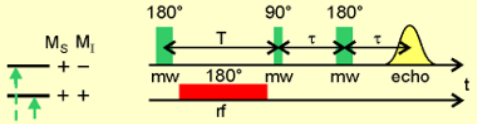

Mims ENDOR

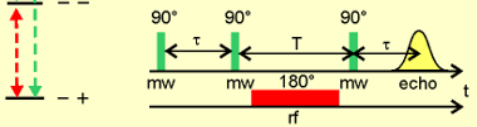

hfc and nqc determination

CW EPR
Pulse EPR
Multiresonance Techniques

Photosynthetic Process

$$2H_2A + CO_2 \xrightarrow[\text{BChl}]{h\nu} (CH_2O) + H_2O + 2A$$

'sugar'

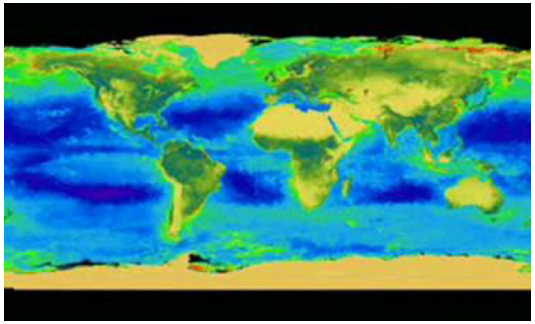

Reaction center of purple bacteria from *Rhodobacter sphaeroides*

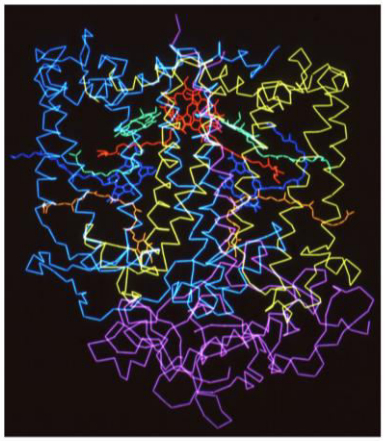

Cofactor arrangement

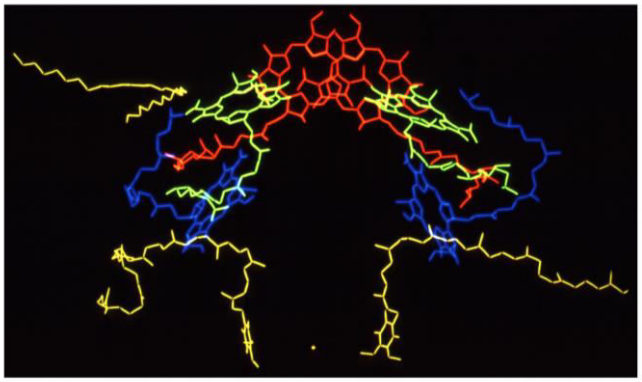

Allen et al. Proc. Natl. Acad. Sci. 1987, 84, 6162

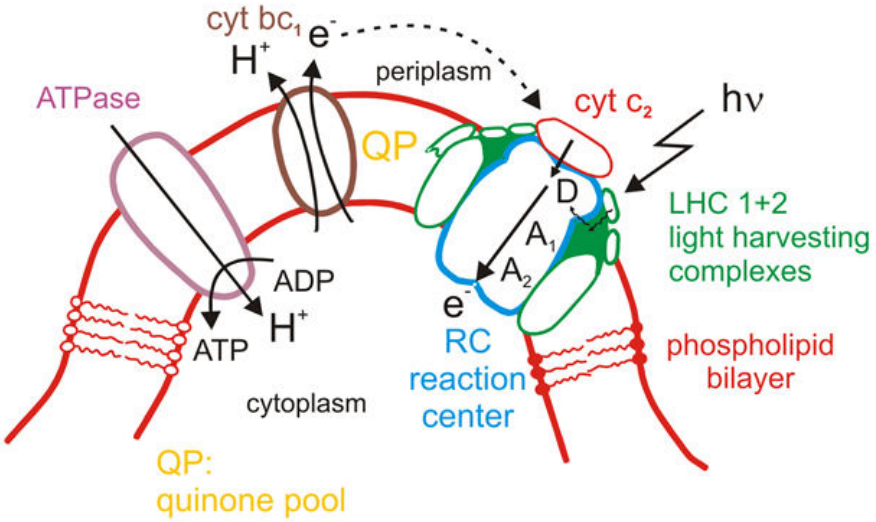

The photosynthetic machinery

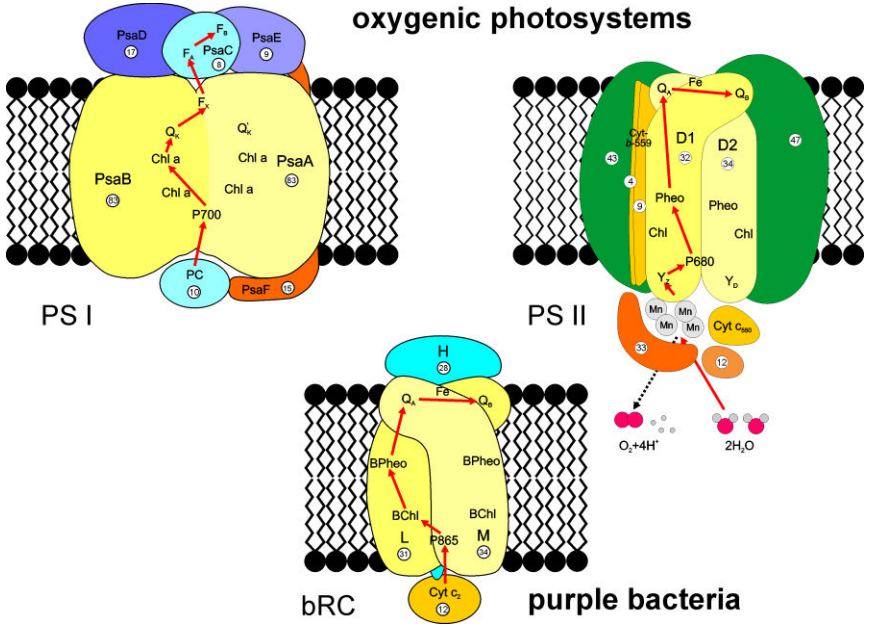

Paramagnetic Species in the Photosynthetic Proteins

Primary reactions in Photosynthesis

$$PIQ_AFe^{II}Q_B \xrightarrow{h\nu} P^*IQ_AFe^{II}Q_B \rightarrow P^{+}I^{-}Q_AFe^{II}Q_B \rightarrow P^{+}IQ_A^{-}Fe^{II}Q_B \rightarrow P^{+}IQ_AFe^{II}Q_B^{-}$$

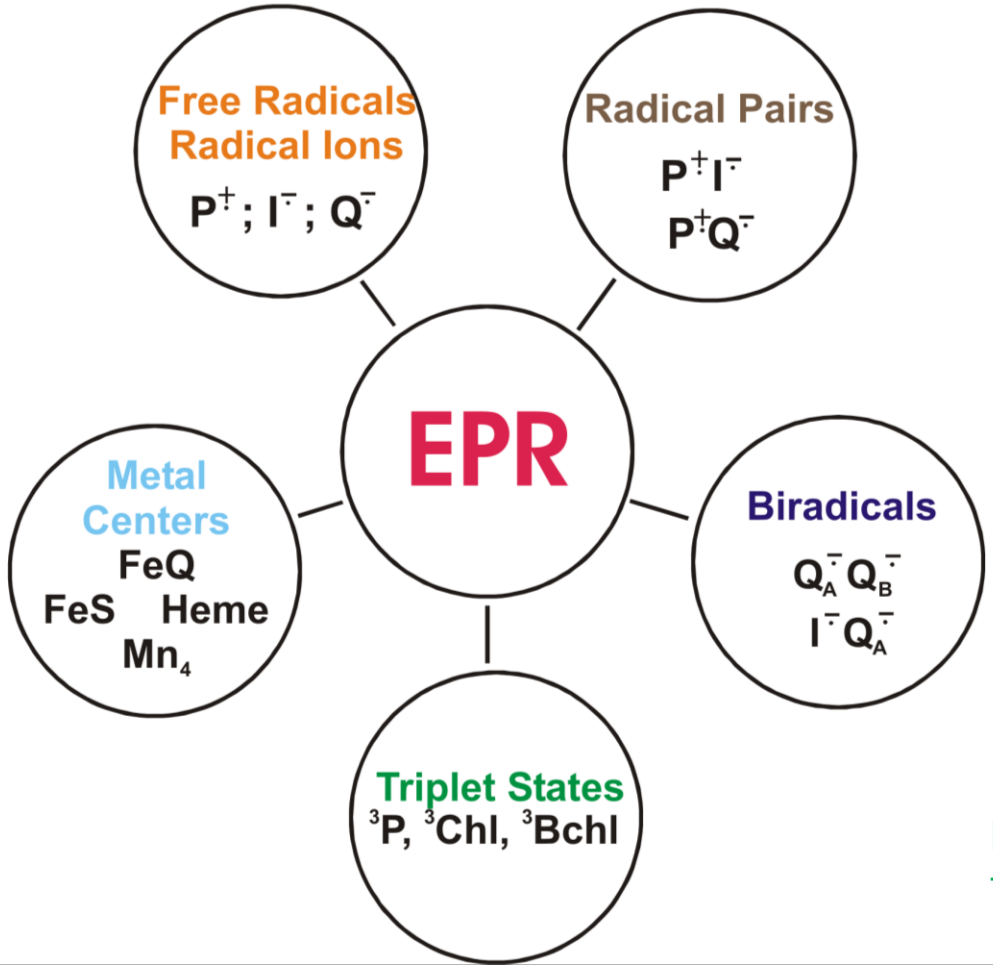

Photosynthesis:
the garden of Eden for EPR spectroscopy!

A Plethora of Radicals

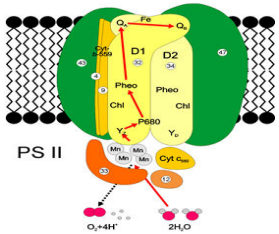

Identification of radical species, light-induced or chemically oxidized in Photosystem II, by CW-EPR and High-Field EPR

9 GHz / 0.3 T

285 GHz / 10 T

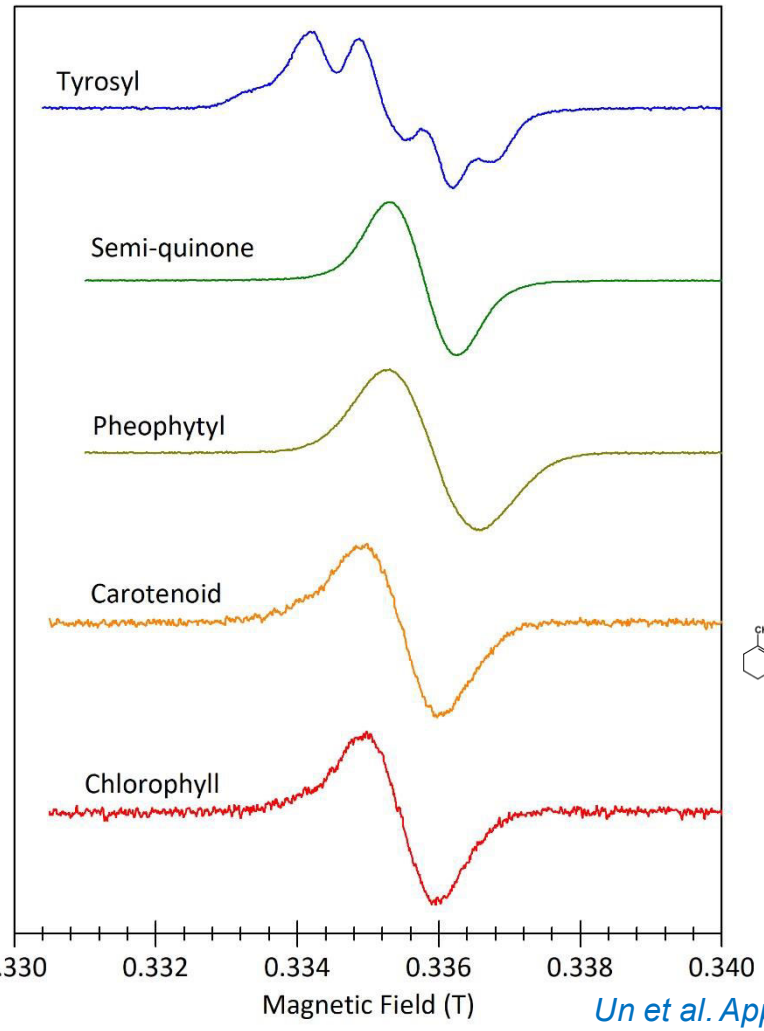

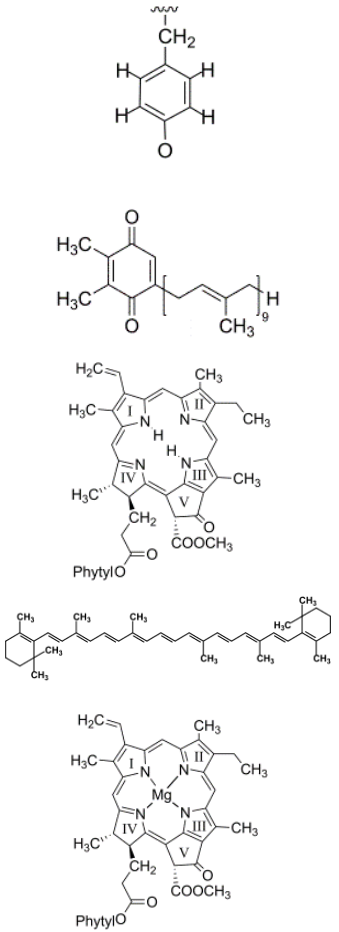

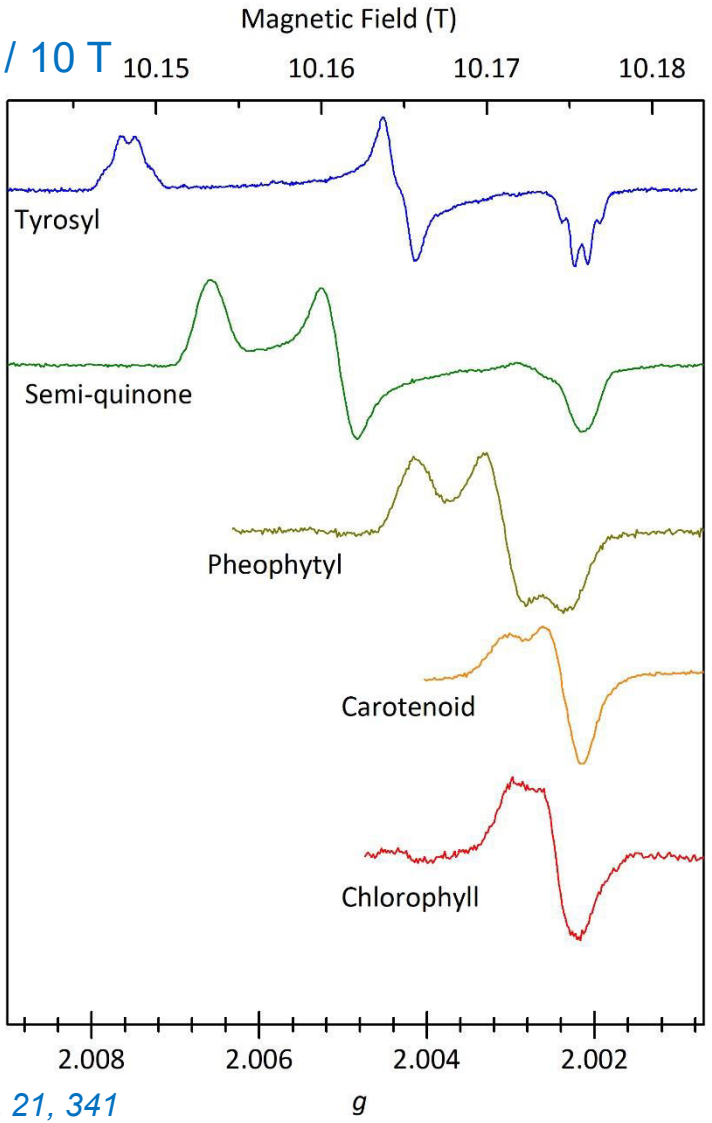

Un et al. Appl. Magn. Reson. 2001, 21, 341

94 GHz EPR of the Tyrosyl Radical in Photosystem II Single Crystals

Single crystal of Photosystem II from *S. elongatus*

4PS II dimers/unit cell
space group $P2_1\,2_1\,2_1$

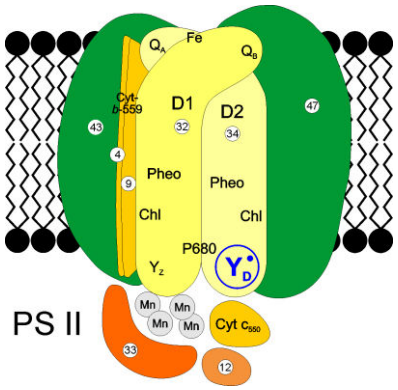

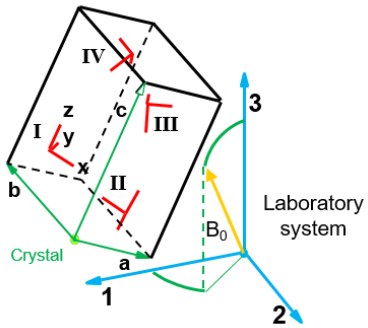

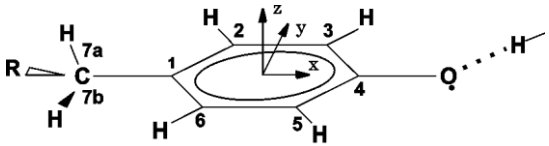

Tyrosyl $Y_D^{\bullet}$

$g_x = 2.00767$ $g_y = 2.00438$ $g_z = 2.00219$

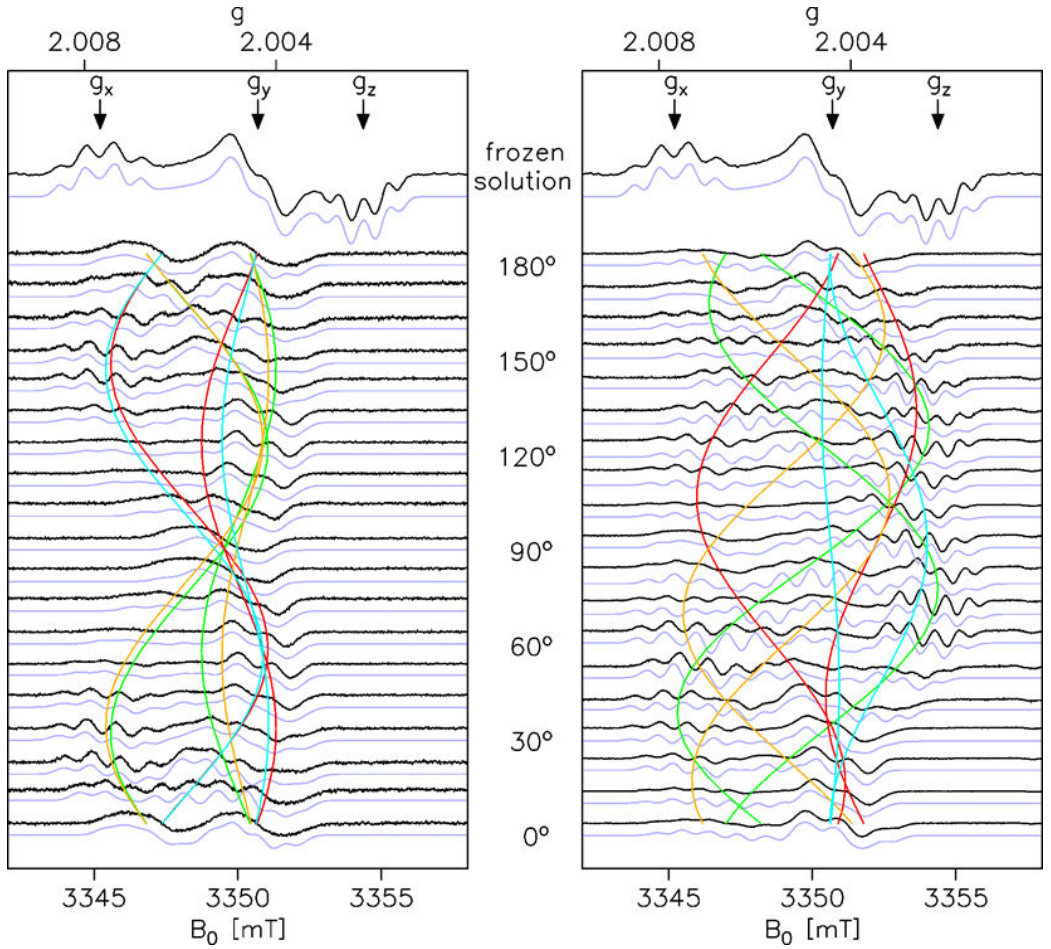

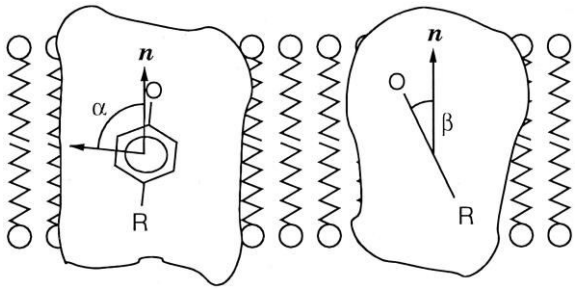

Orientation of the phenoxyl group of $Y_D^{\bullet}$ with respect to the membrane normal as derived from the single-crystal EPR spectra

Hofbauer et al., Proc. Natl. Acad. Sci. 2001, 98, 6623
Dorlet et al., Biochemistry 2000, 39, 7826

94 GHz EPR on Quinone Radicals in Bacterial Reaction Centers

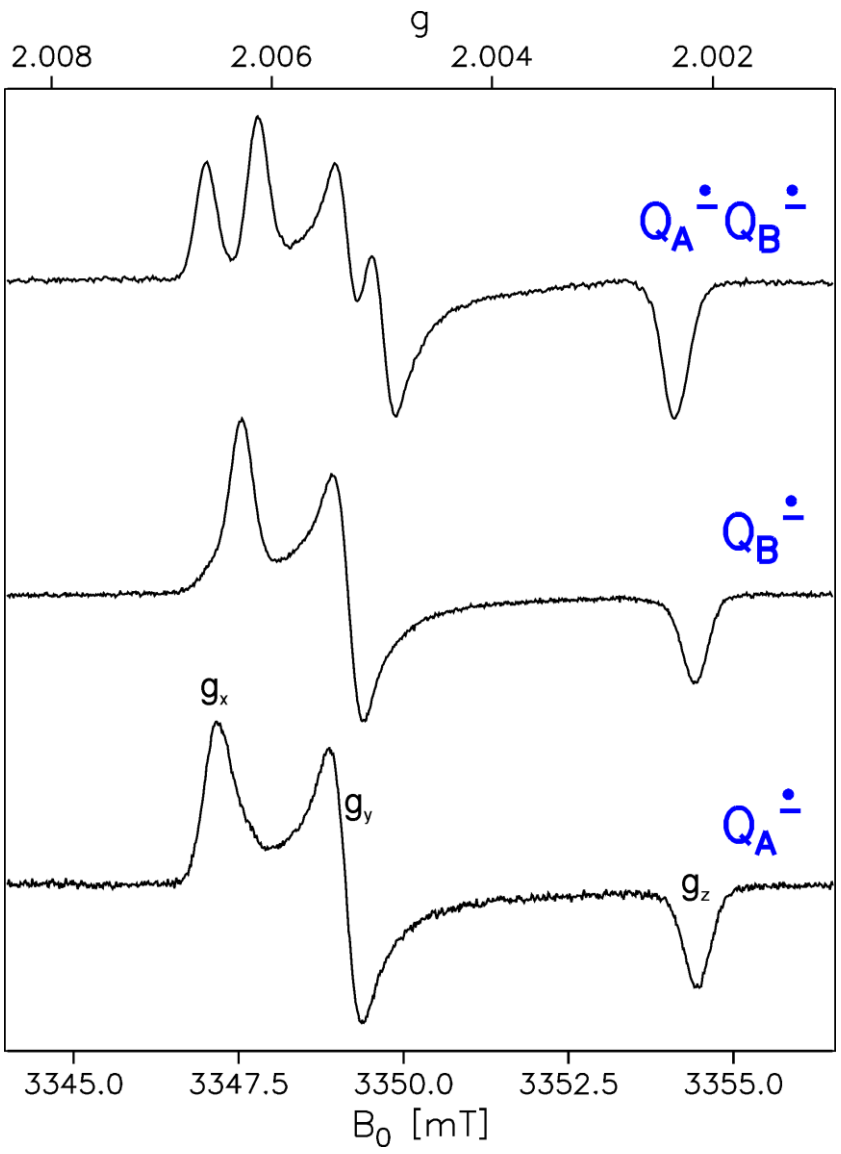

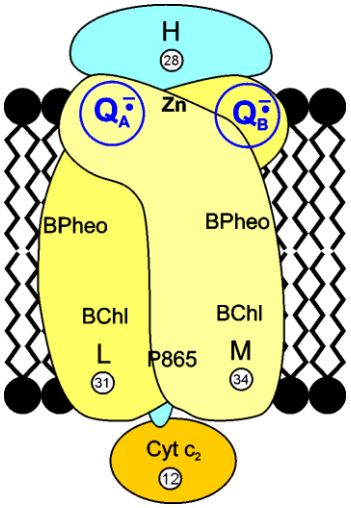

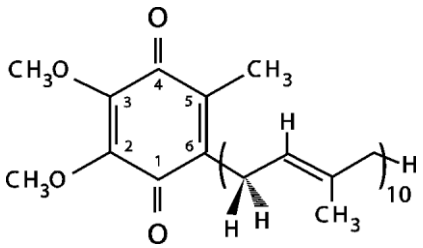

Q_A, Q_B

Reaction Centers from *Rhodobacter sphaeroides*

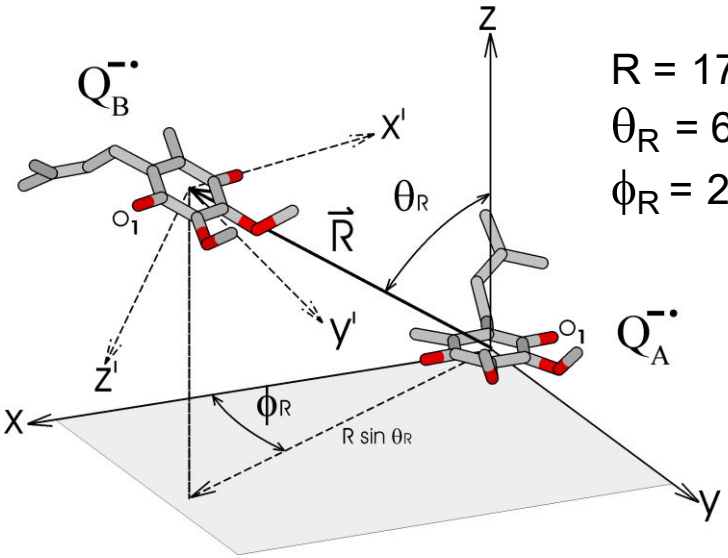

R = 17.2 Å

θ_R = 65°

ϕ_R = 2°

Calvo et al. J. Am. Chem. Soc. 2000, 122, 7327

Primary Donor: the Special Pair

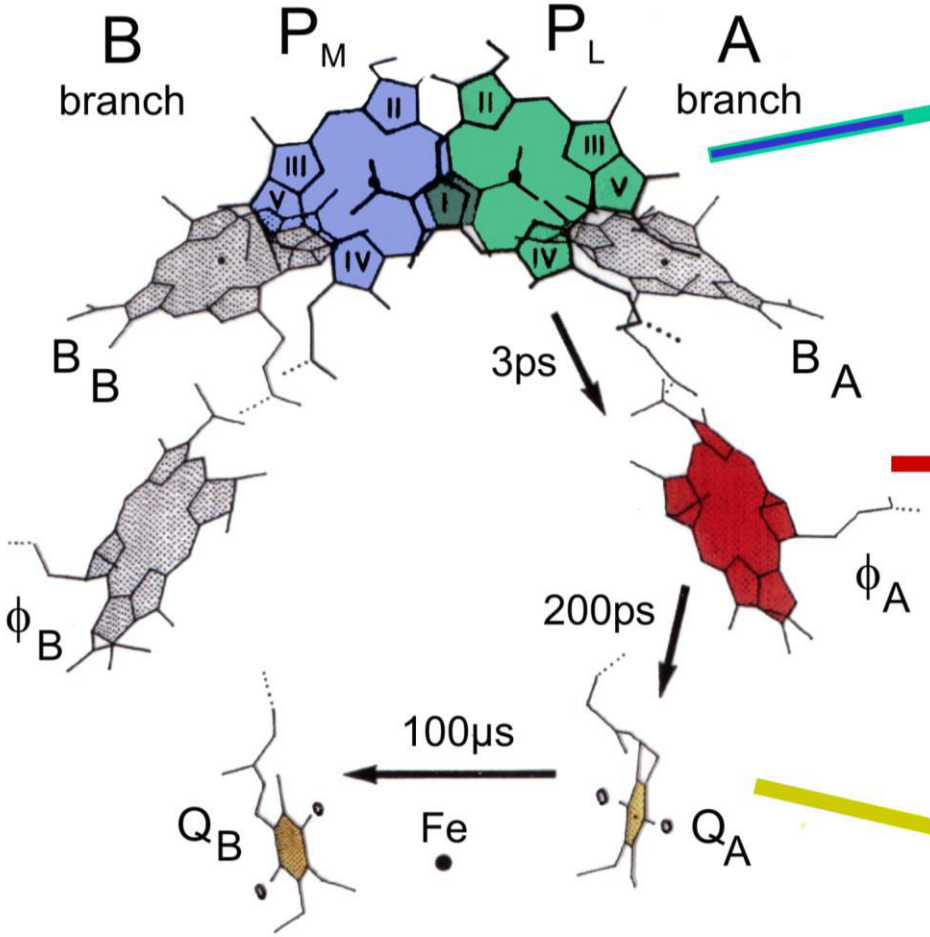

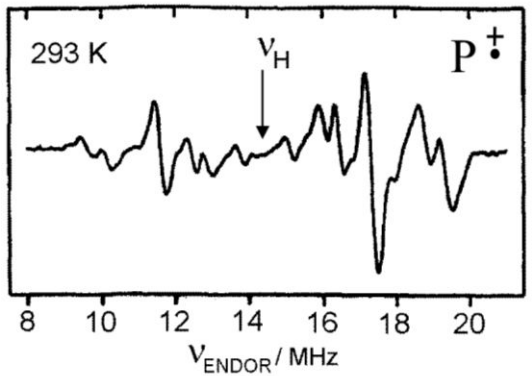

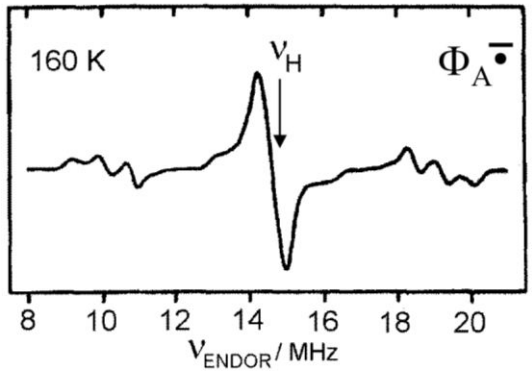

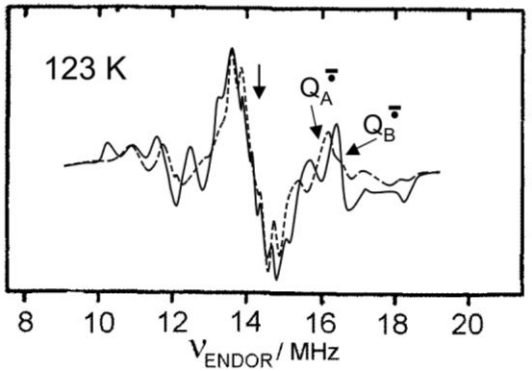

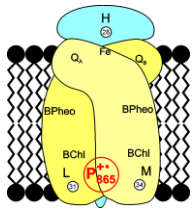

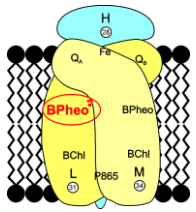

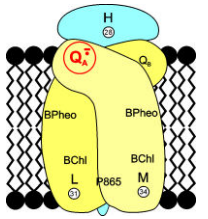

Reaction center of *Rhodobacter sphaeroides*

Lubitz W. and Lendzian F. (1996) ENDOR Spectroscopy. In: Amesz J., Hoff A.J. (eds) Biophysical Techniques in Photosynthesis. Advances in Photosynthesis and Respiration, vol 3. Springer, Dordrecht

$$\nu_{ENDOR} = |\nu_H \pm A/2|$$

Hyperfine Couplings: ENDOR and TRIPLE in Solution

BChl *a* $^{+\bullet}$ (CH_2Cl_2/CH_3OH, Iodine, 255K)

$$\nu^{\pm}_{ENDOR} = \left| \nu_n \pm \frac{A}{2} \right|$$

ENDOR

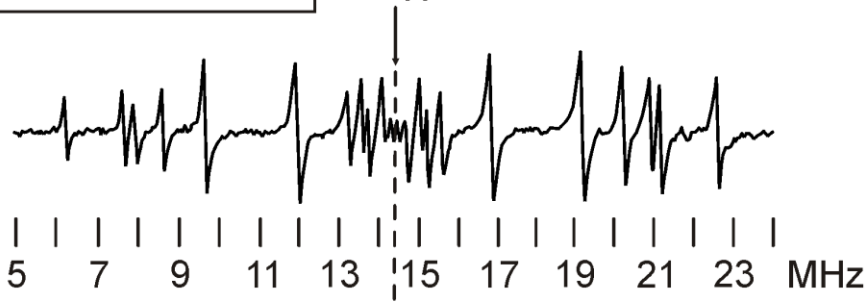

Special TRIPLE

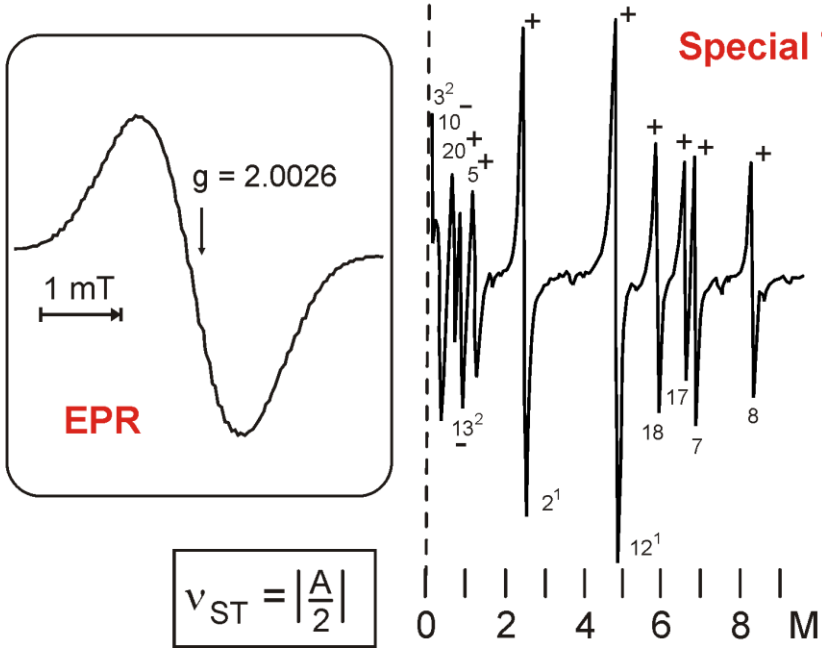

$$\nu_{ST} = \left| \frac{A}{2} \right|$$

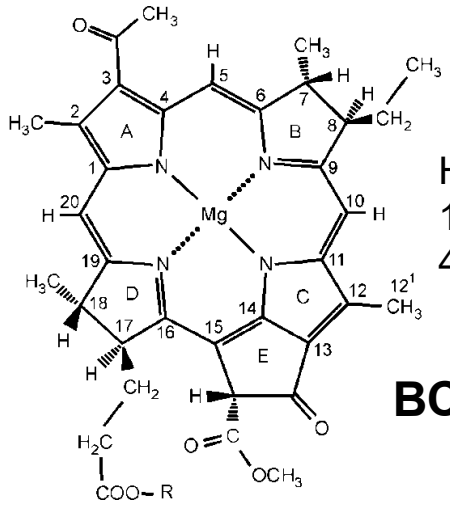

Hyperfine couplings:
12 protons
4 nitrogens

BChl *a*

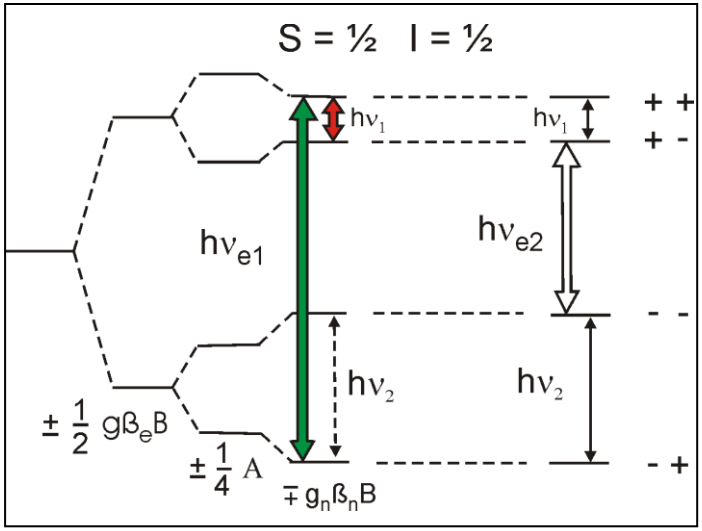

Lubitz et al. Appl. Magn. Reson. 1997, 13, 531

Primary Donor Cation Radical of Bacterial Reaction Center

Primary donor radical cation $\mathbf{P_{865}^{+\bullet}}$ in the reaction center of *Rb. sphaeroides*

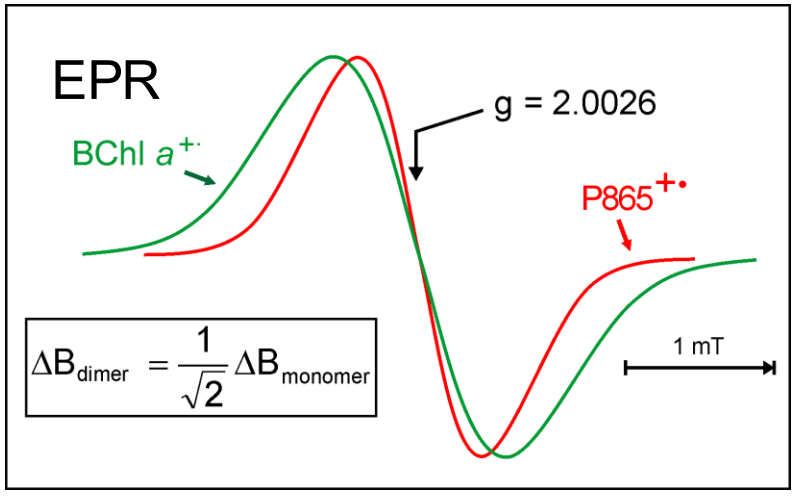

Norris et al. Proc. Natl. Acad. Sci. 1971, 68, 625

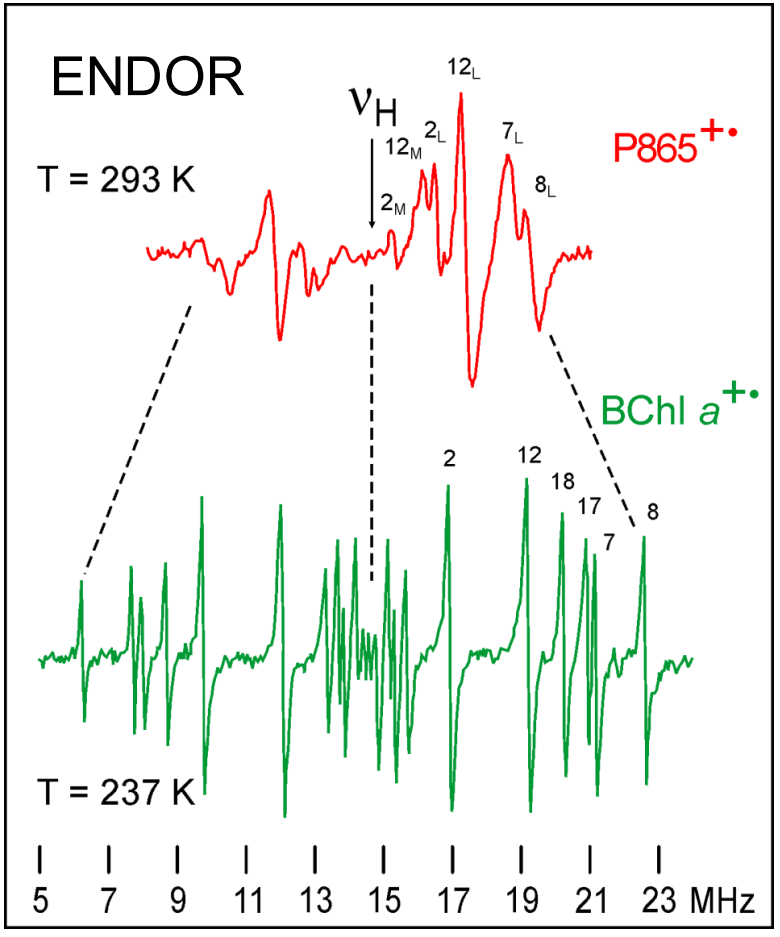

Lubitz et al. Appl. Magn. Reson. 1997, 13, 531

Comparison between experimental and calculated spin densities

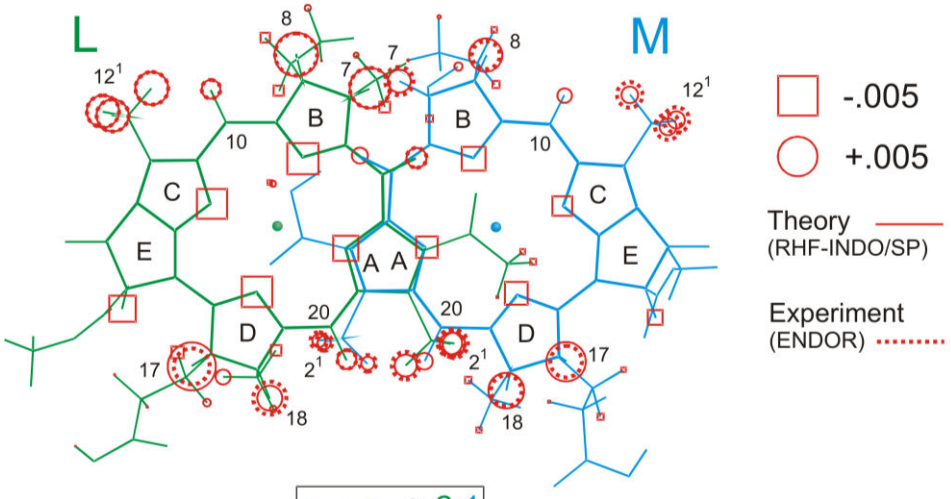

$\rho_L : \rho_M \cong 2:1$

$$A_{dimer} = \frac{1}{n} A_{monomer}$$

n = 2 → sym. dimer

n ≠ 2 → asym. dimer

Plato et al. in "Chlorophylls," H. Scheer, ed., CRC Press, Boca Raton (1991)

Effects of Axial Ligation on the ENDOR spectrum of the Primary Donor

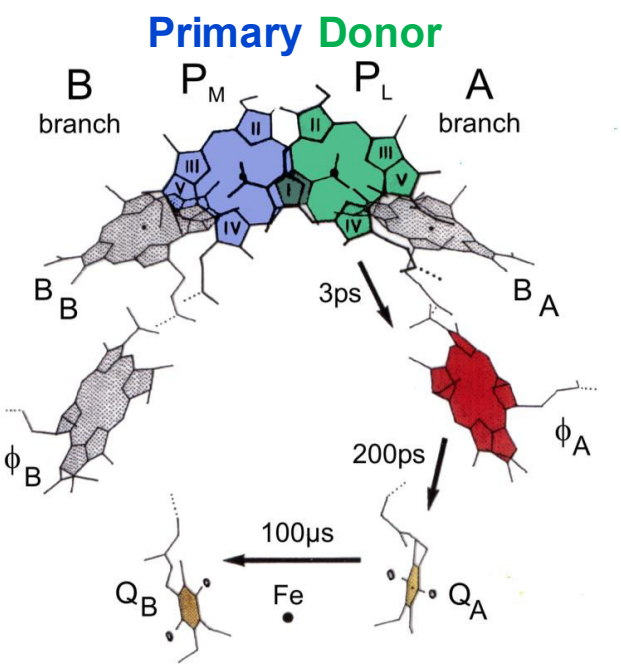

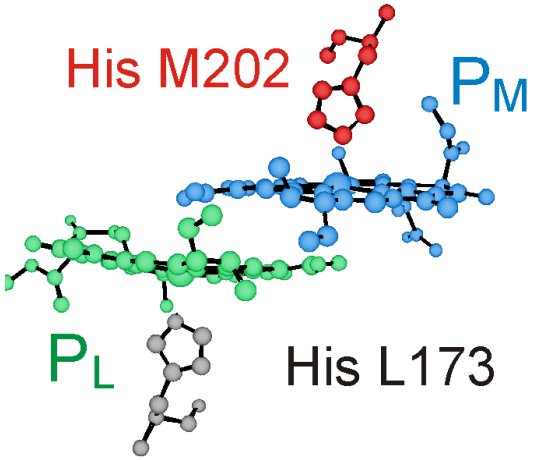

Primary donor radical cation $\mathbf{P_{865}^{+\bullet}}$ in the reaction center of *Rb. sphaeroides*

Midpoint Potentials

system / mutant	donor midpoint potential E_P^{ox} / mV	P^+ spin density ρ_L
wild type	504 ± 5	0.68
HE(M202)	673 ± 10	~ 1
BChl *a*	660 ± 10	1

X-band TRIPLE ENDOR spectra in solution

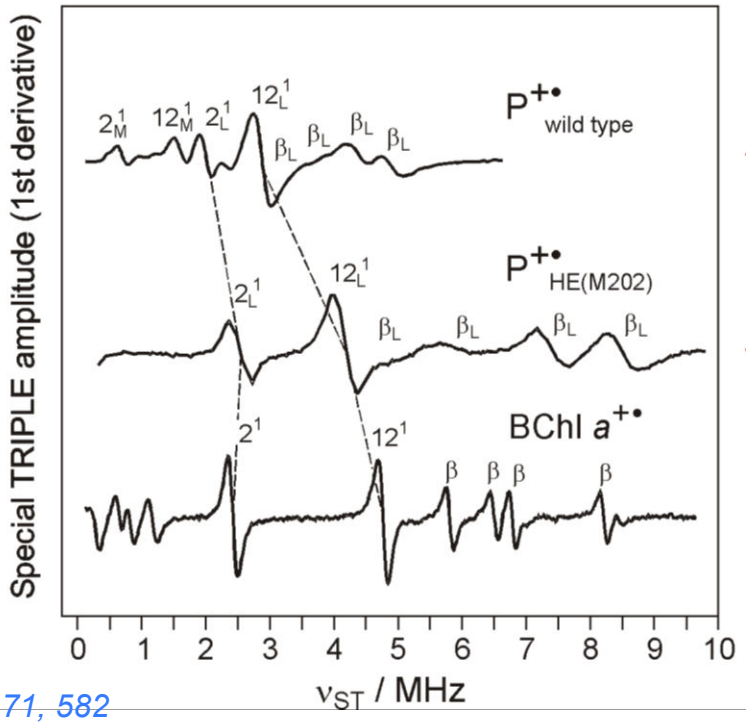

M202 mutant

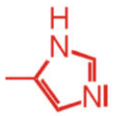

His (H)

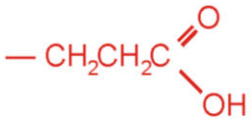

Glu (E)

—

Nabedryk et al. Photchem. Photobiol. 2000, 71, 582

Effects of Axial Ligands and Hydrogen Bonding on the Spin Distribution

Relation midpoint potential and spin distribution

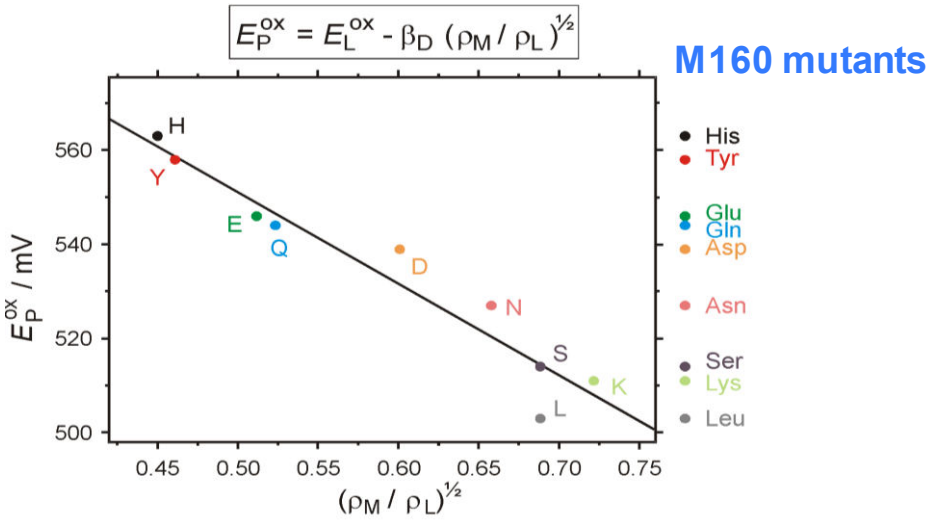

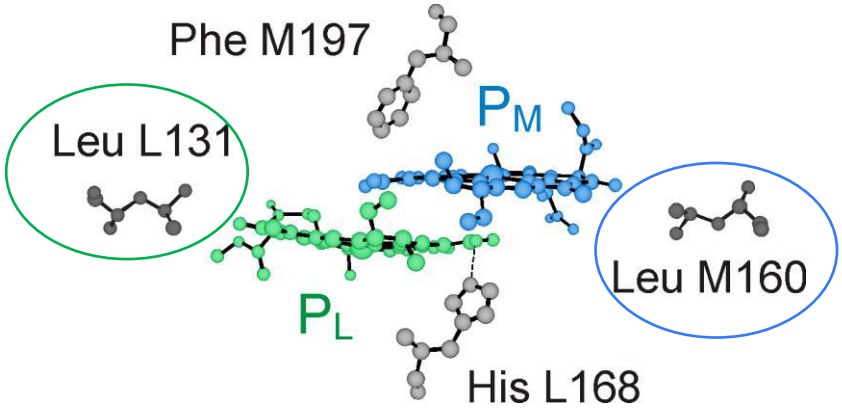

Electronic Structure

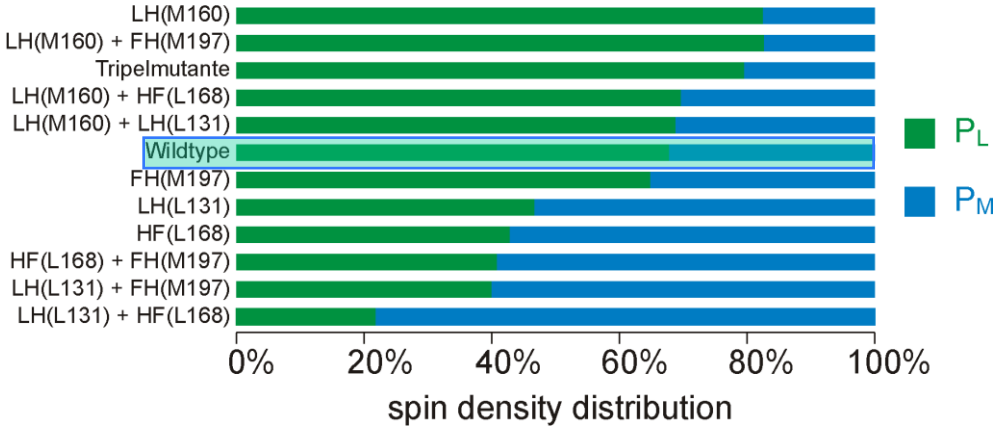

Effects of Hydrogen Bonding to the acetyl and keto groups:

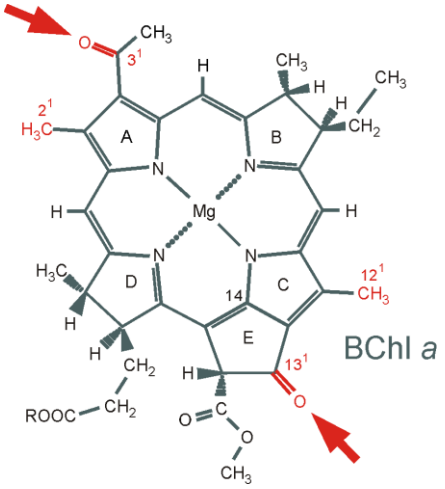

All mutants perform ET, tuning of the electronic properties by the protein surroundings

Müh et al. Phys. Chem. B 2002, 106 ,3226

Comparison between Photosynthetic Primary Donor Radicals

Density-functional theory calculations on the primary donor cation radical of bacterial reaction centers

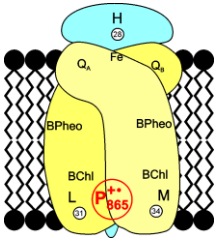

BChl $a^{+\bullet}$

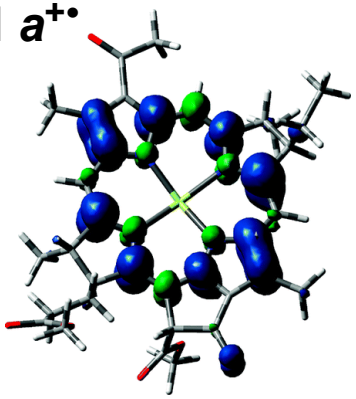

Spin density

$P_{865}^{+\bullet}$

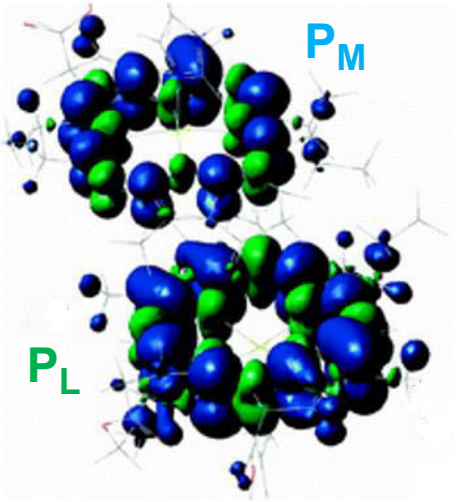

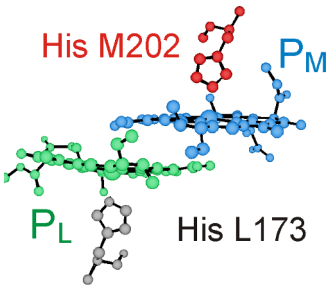

Robotham et al. Biochemistry 2008, 47, 13261

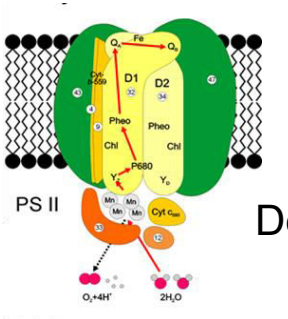

Density-functional theory calculations on the primary donor cation radical of PS II

X-band CW-ENDOR 80K

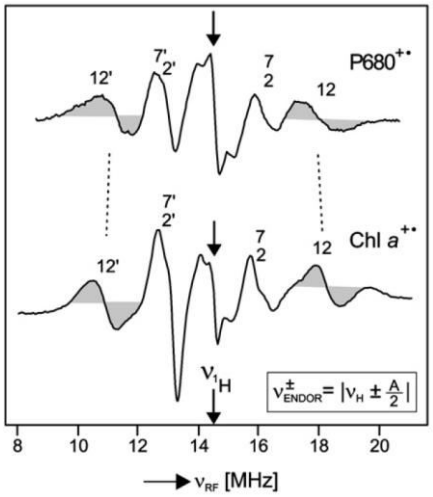

Chl $a^{+\bullet}$

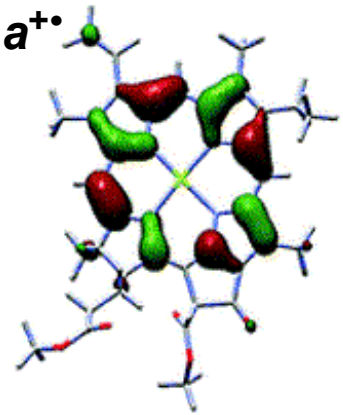

SOMO

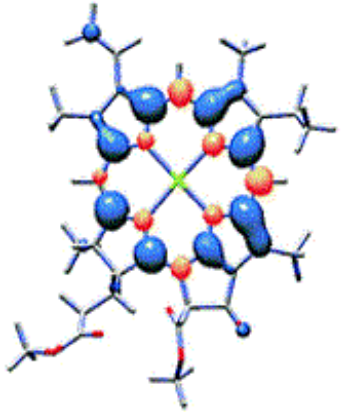

Spin density

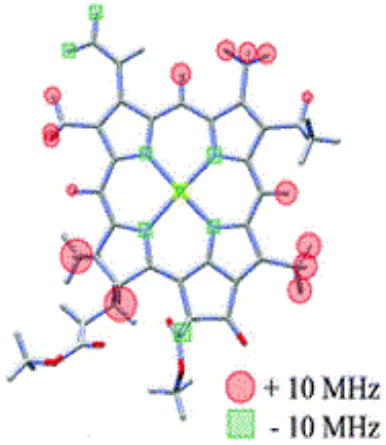

Isotropic hfcs

Lubitz Phys. Chem. Chem. Phys., 2002, 4, 5539

Inter-System Crossing

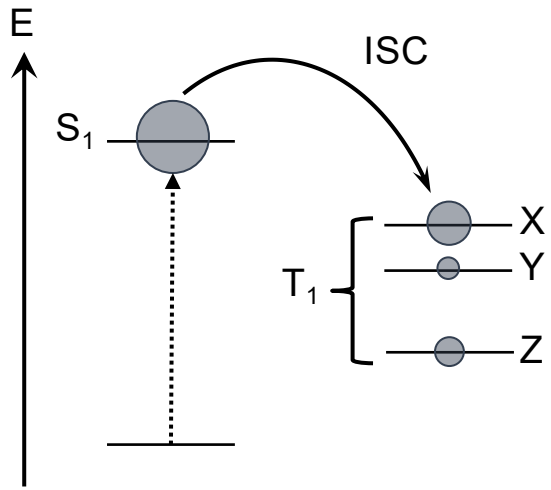

Triplet State

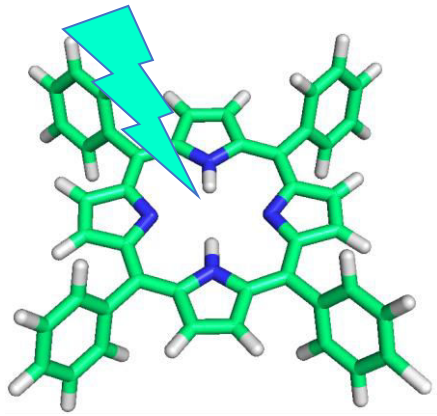

^{T}Chl

Photoinduced Electron Transfer

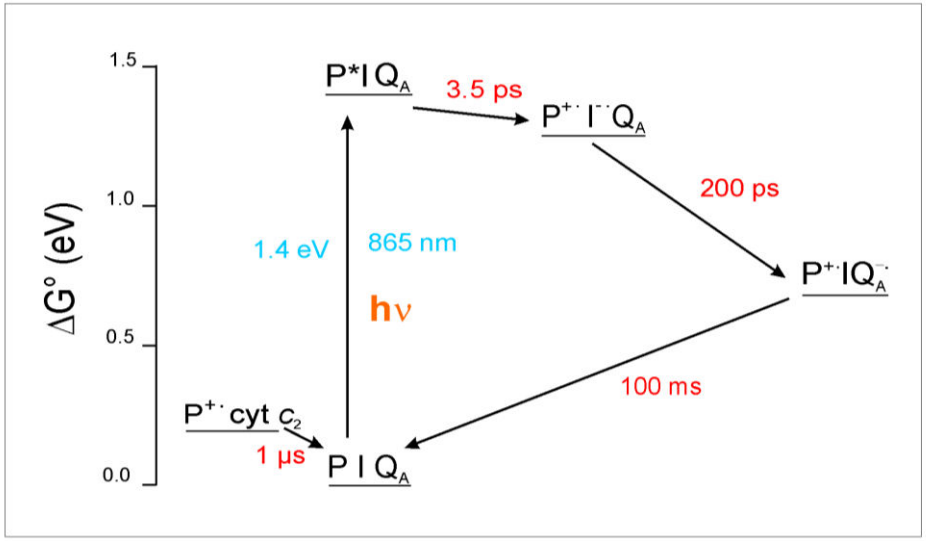

BChl a·+

Spin-Correlated Radical Pair

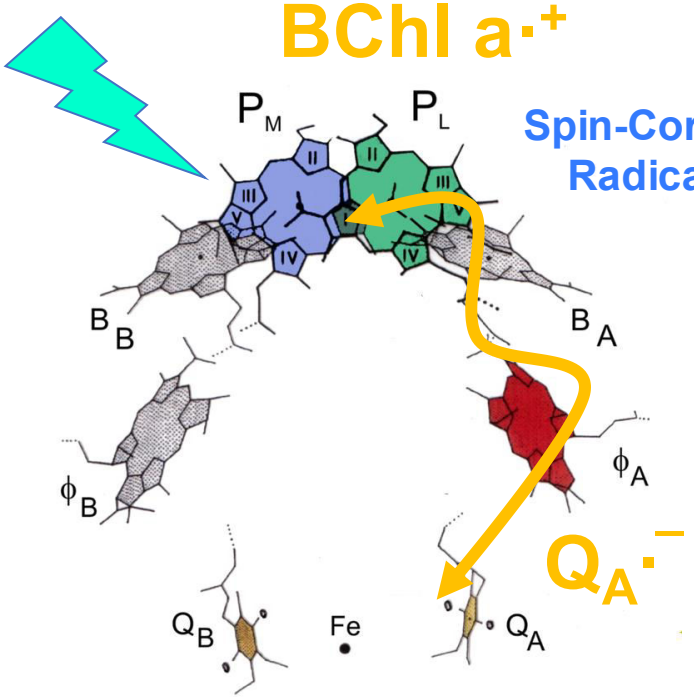

Time-Resolved EPR Techniques coupled to Photoexcitation

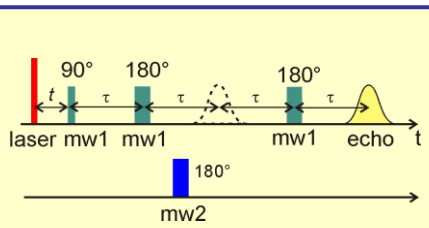

LiDEER/PELDOR

Distance measurements
Triplet states

Transient EPR

ZFS-Tensors
Kinetics

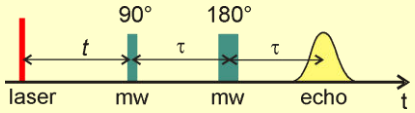

Pulse (HF) EPR

g-, ZFS-Tensors
Kinetics

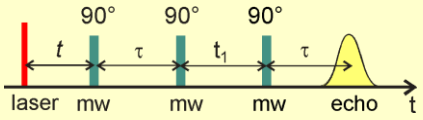

ESEEM/ HYSCORE

Hyperfine-, Quadrupole-Tensors

Dynamics Kinetics
EPR
Triplets, Biradicals
Radical pairs
Electr. Structure Distances Orientations

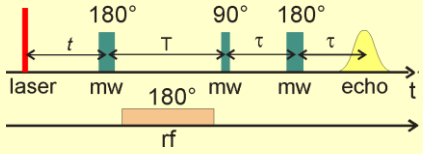

Pulse ENDOR

Hyperfine-, Quadrupole-Tensors

The Ricombination Triplet State in Photosytem II

$$PIQ_A^{red} \xrightarrow{h\nu} {}^1P^*IQ_A^{red} \xrightarrow[ps]{} {}^1(P^+I^-)Q_A^{red} \underset{ns}{\overset{\omega}{\rightleftharpoons}} {}^3(P^+I^-)Q_A^{red} \xrightarrow[ns]{} {}^3PIQ_A^{red} \xrightarrow[\mu s\text{-}ms]{decay}$$

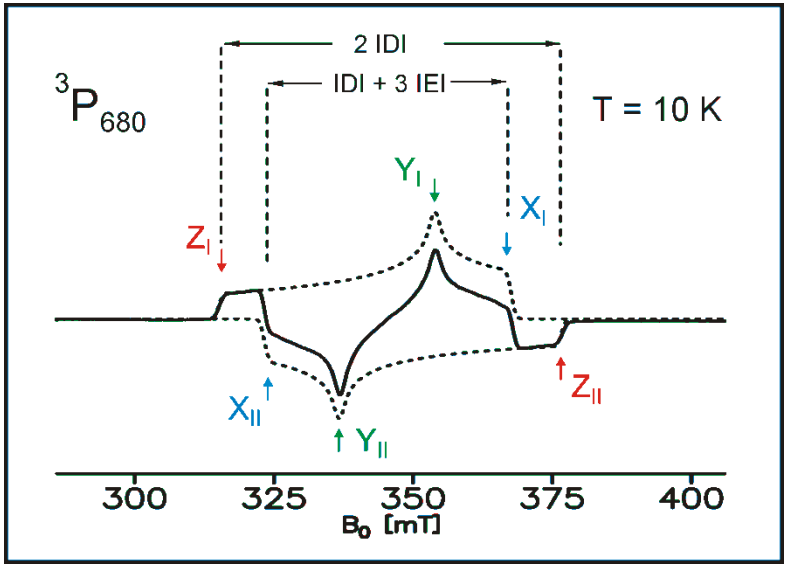

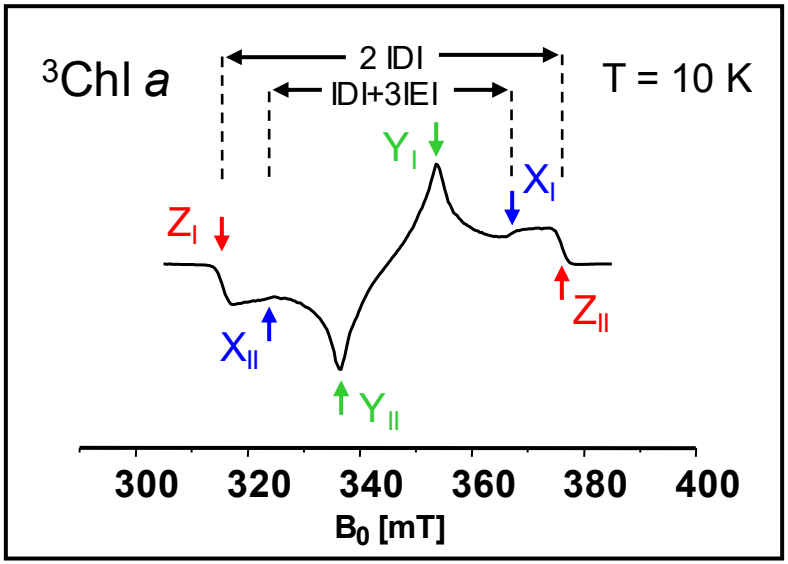

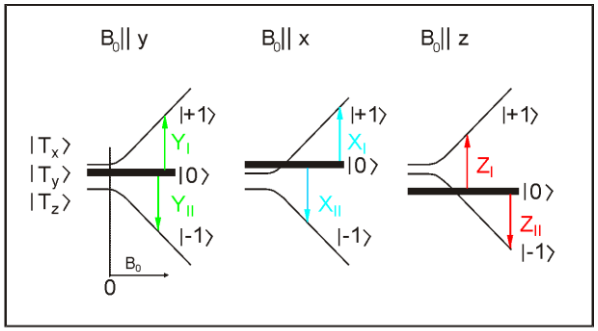

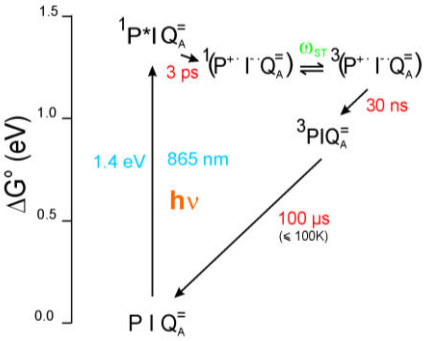

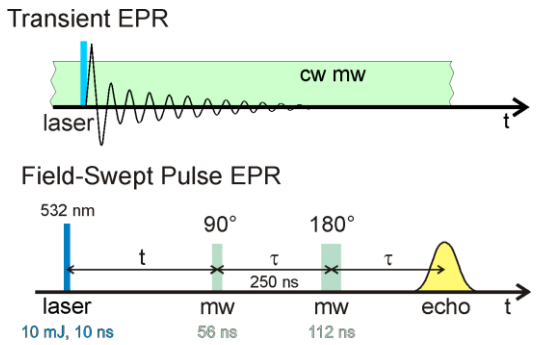

The Zero Field Splitting parameters |D| and |E| reflect the spatial extension and symmetry of the HOMO and LUMO

	^{3}P680	^{3}Chl*a*
IDI	287 x 10^{-4} cm^{-1}	282 x 10^{-4} cm^{-1}
IEI	43 x 10^{-4} cm^{-1}	38 x 10^{-4} cm^{-1}

At low temperatures **^{3}P680** is localized on a *monomeric* Chl a

Lendzian et al., Biochim. Biophys. Acta 2003, 1605,35

Chlorophyll Triplet State in Photosytem II Single Crystals

Transient EPR

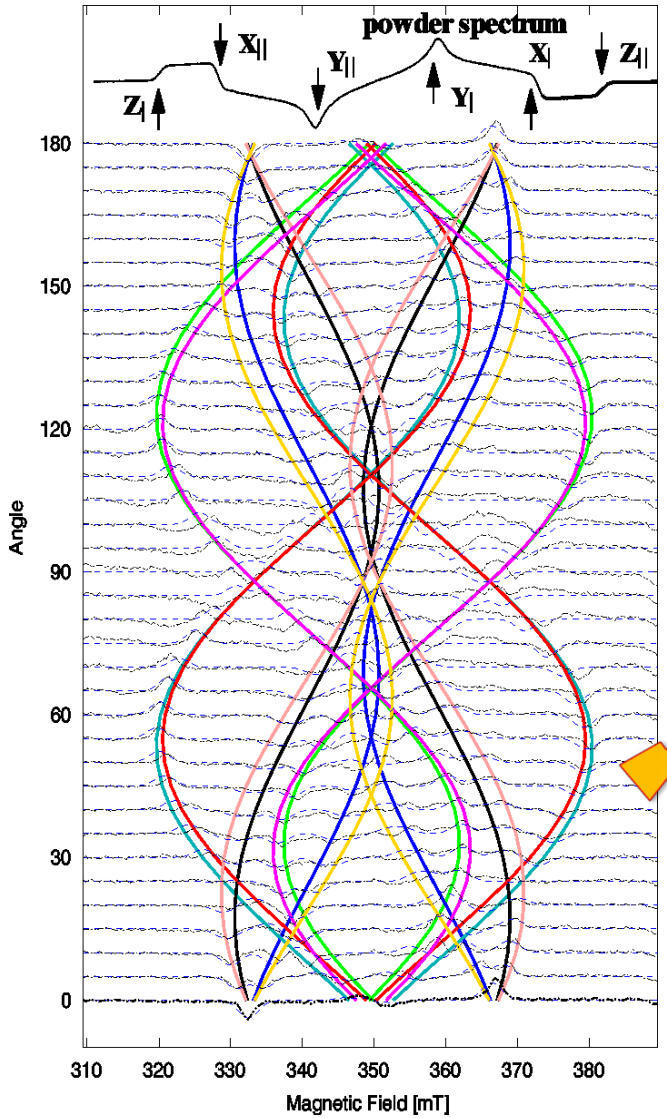

Kammel et al. BBA 2003, 1605,47

Photosystem II **single crystals** of *Synechococcus elongatus:*

Space group $P2_12_12_1$

4 PS II dimers/unit cell

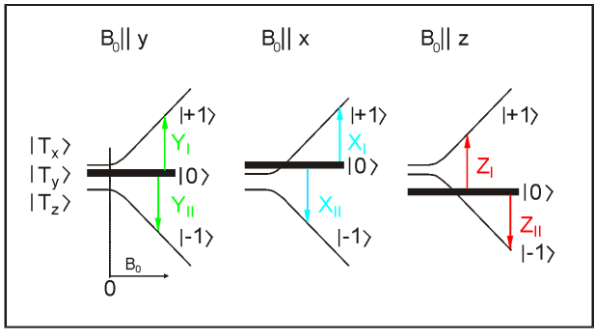

Triplet Zero Field Splitting tensor orientation in the PS II structure

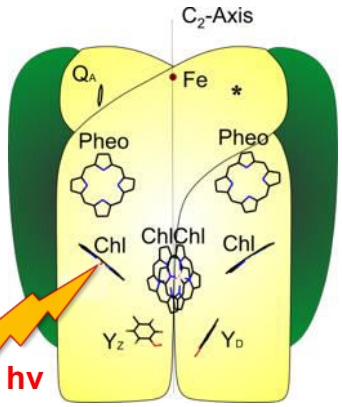

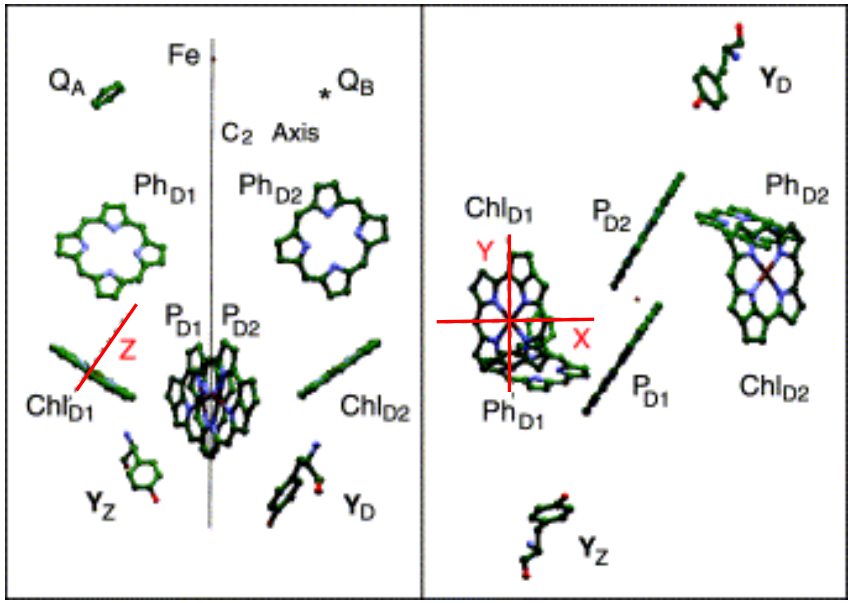

→ The triplet is not localized on the ChlChl pseudo-dimer but on the **monomeric accessory chlorophyll**

The Ricombination Triplet State in *Rb. sphaeroides* Reaction Center

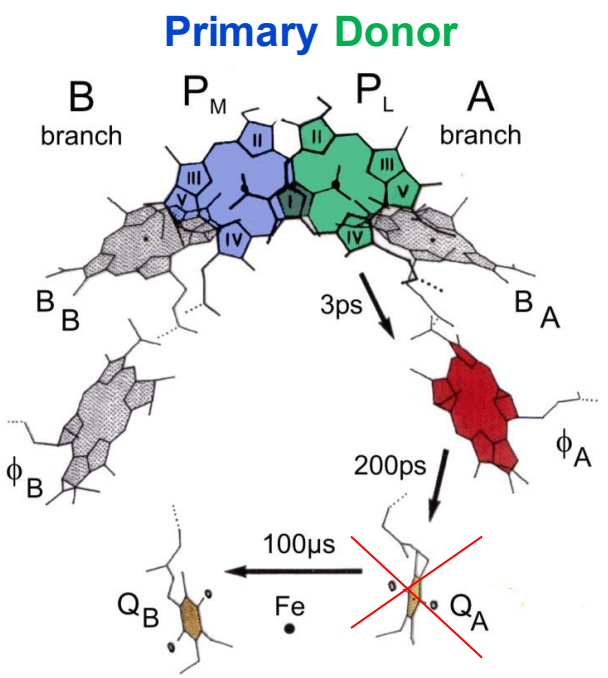

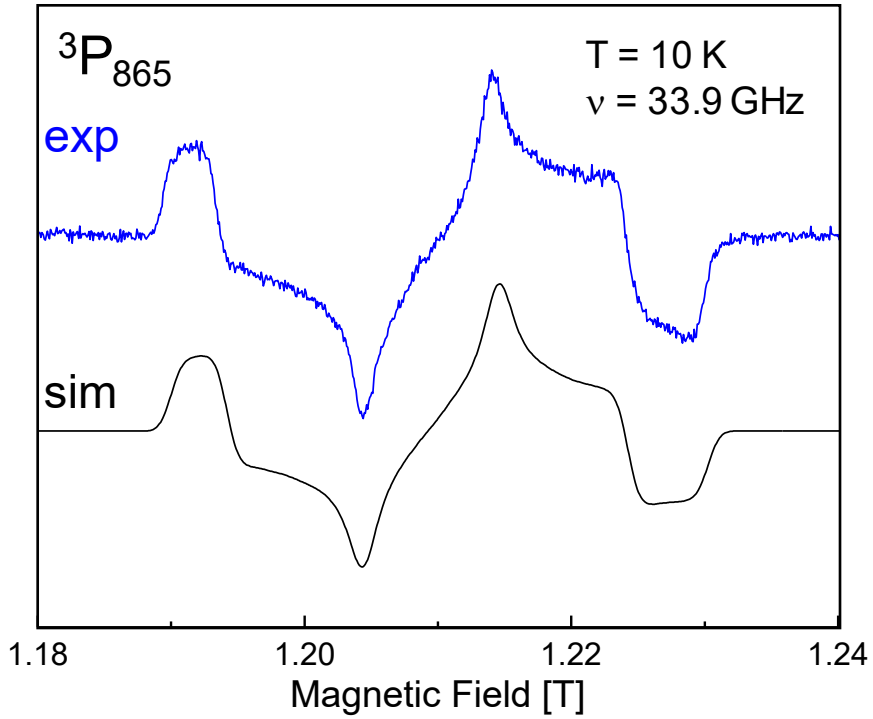

Triplet Zero Field Splitting parameters

BChl *a* dimer $^3P_{865}$ in *Rb. sphaeroides* 2.4.1

D = +0.0188 cm^{-1}
E = +0.0031 cm^{-1}

^{3}BChl *a* monomer

D = +0.0238 cm^{-1}
E = +0.0069 cm^{-1}

The D and E parameters indicate triplet delocalization in the dimer for bacterial reaction center

Marchanka et al. Photosynth Res 2014,120, 99.

Comparison between the Recombination Triplets by Pulse ENDOR

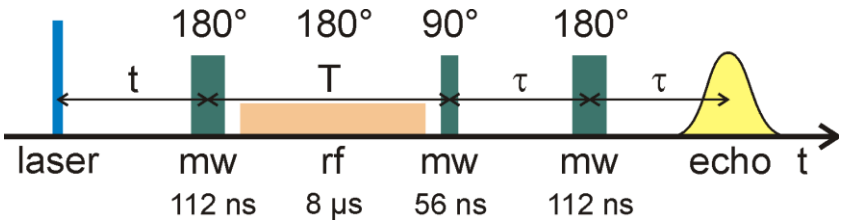

$$\nu_{ENDOR} = | \nu_n - M_S A_{ii}^T |$$

Davies ENDOR at X-band

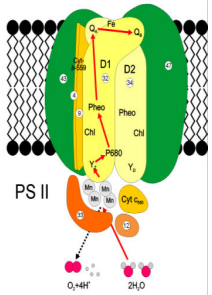

Triplet on a monomeric Chl *a*

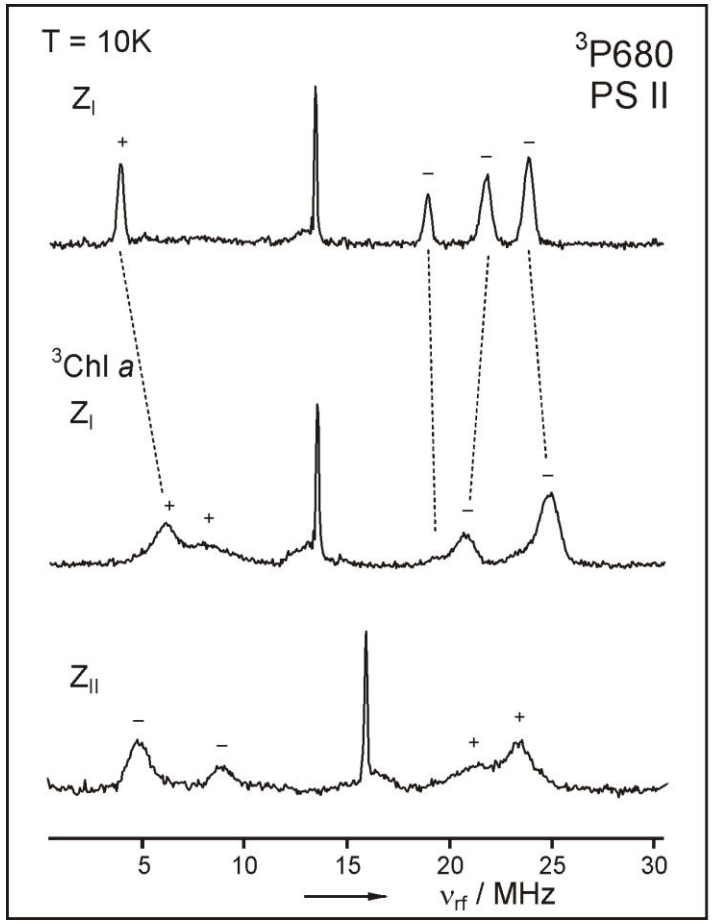

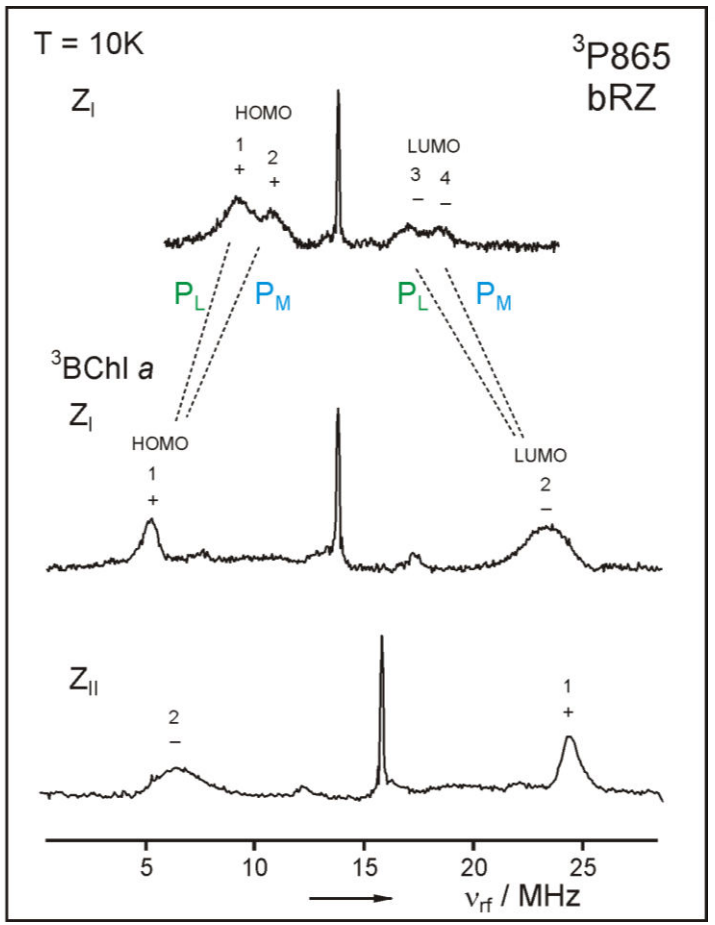

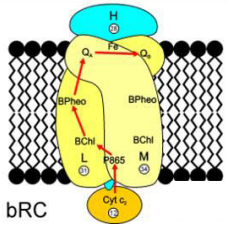

Triplet on the dimer of BChl *a*

$\rho_L:\rho_M=3:1$

Lendzian et al. BBA 2003, 1605, 35

Triplet ENDOR: Information on the Electronic Structure

Density Functional calculations on $^3P_{865,}$ the triplet state of primary donor of bacterial reaction center

P_{865}

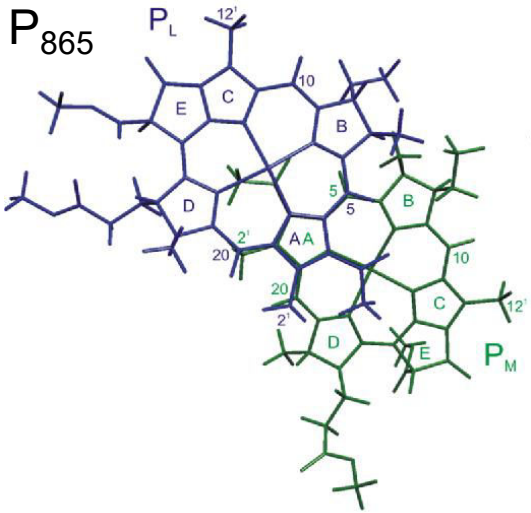

HOMO

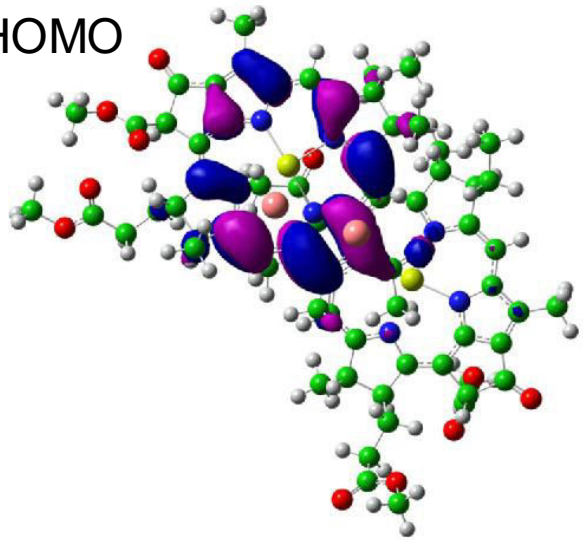

LUMO

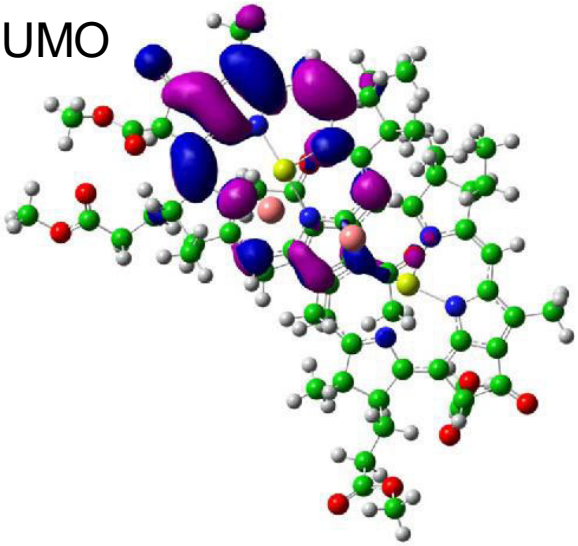

Triplet ENDOR spectroscopy provides information on both the HOMO and LUMO

BChl *a*

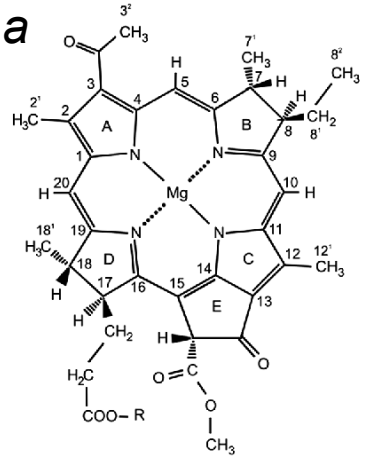

HOMO

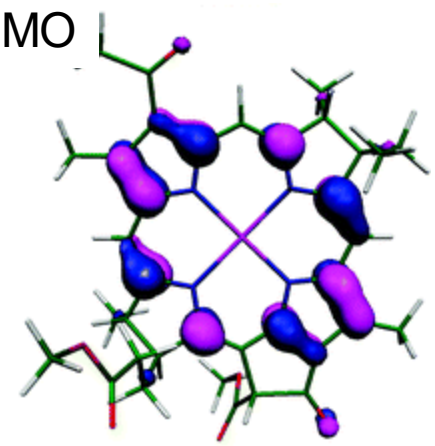

LUMO

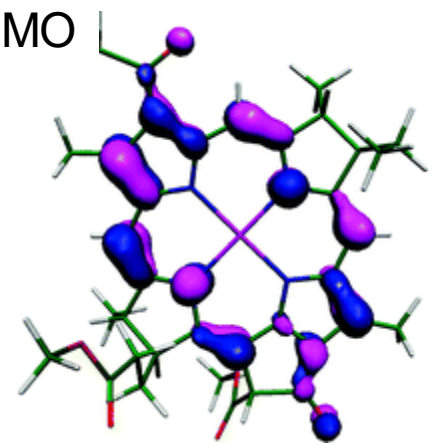

Marchanka et al. J. Phys. Chem. B 2009, 113, 6917

Marchanka et al. Photosynth Res 2014,120, 99.

Out-of-Phase ESEEM of Photoinduced Radical Pairs

Out of Phase ESEEM

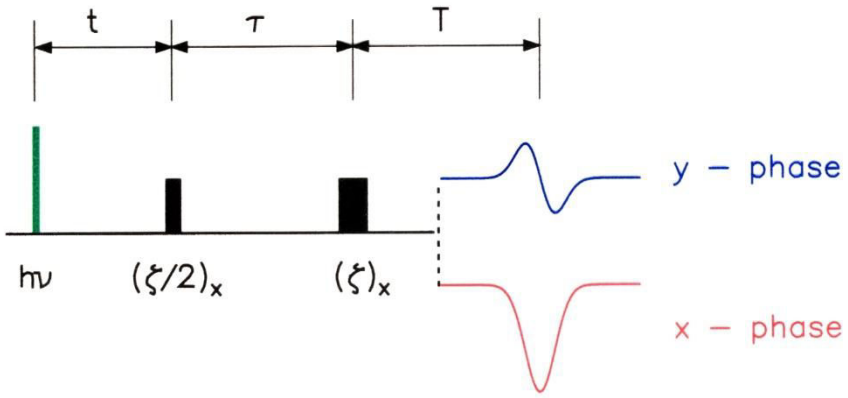

Modulation frequency: $S_{\chi}(\tau) \sim \sin(\Gamma\tau)$

with $\Gamma = 2J - 2D(\cos^2\theta - 1/3)$

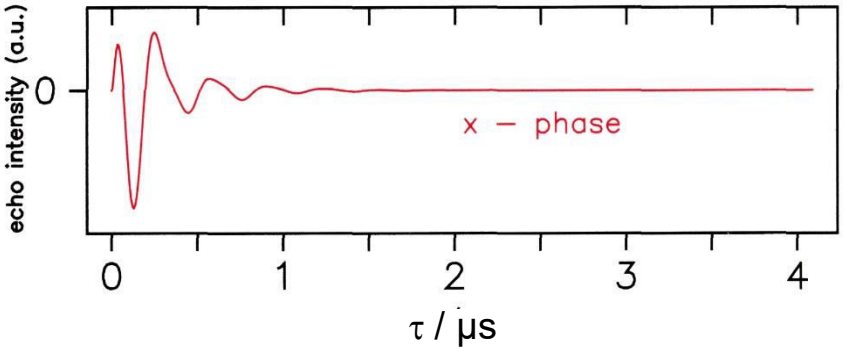

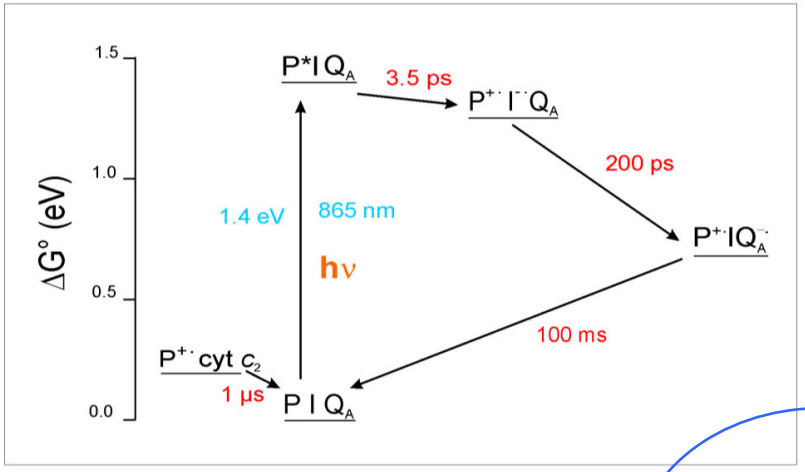

Sine Fourier Transform: $S_{\chi}(\nu) = \pm\delta(\nu_{\pm} \Gamma)$

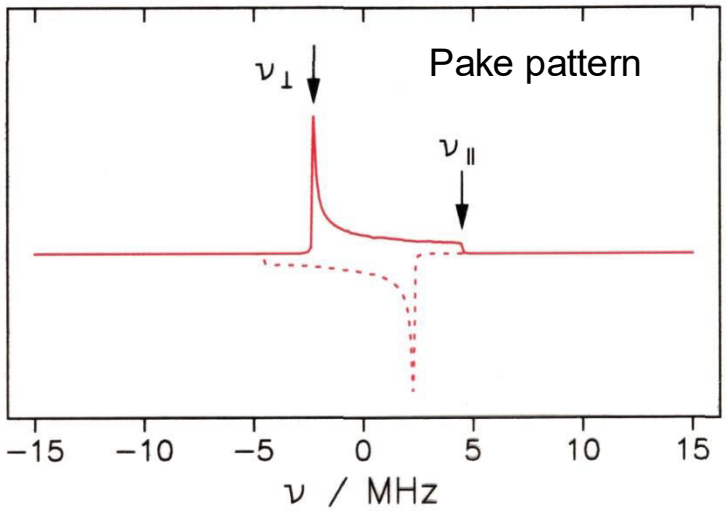

$\nu_{\perp} = \pm 2\,(J + D/3)$

$\nu_{\parallel} = \pm 2\,(J - 2D/3)$

$r \sim -(\frac{1}{D})^{1/3}$

J isotropic exchange parameter
D spin-spin dipolar coupling parameter

Dzuba S.A. and Hoff A.J. (2002) in: Berliner L.J., Eaton G.R., Eaton S.S. (eds) Distance Measurements in Biological Systems by EPR. Biological Magnetic Resonance 2002, vol 19. Springer, Boston, MA

Out-of-Phase ESEEM of Photosynthetic Radical Pairs

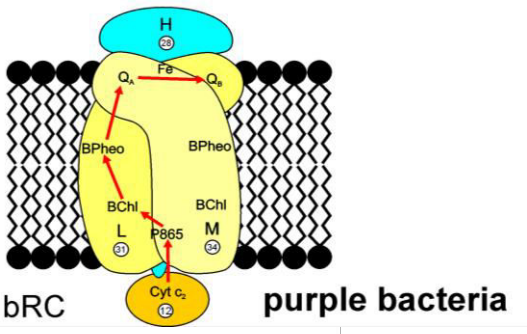

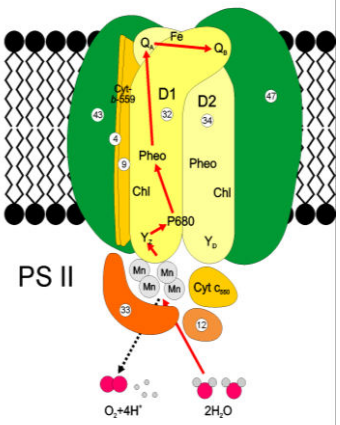

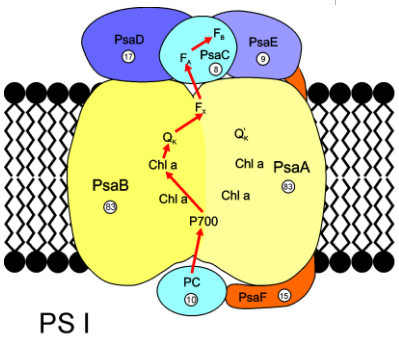

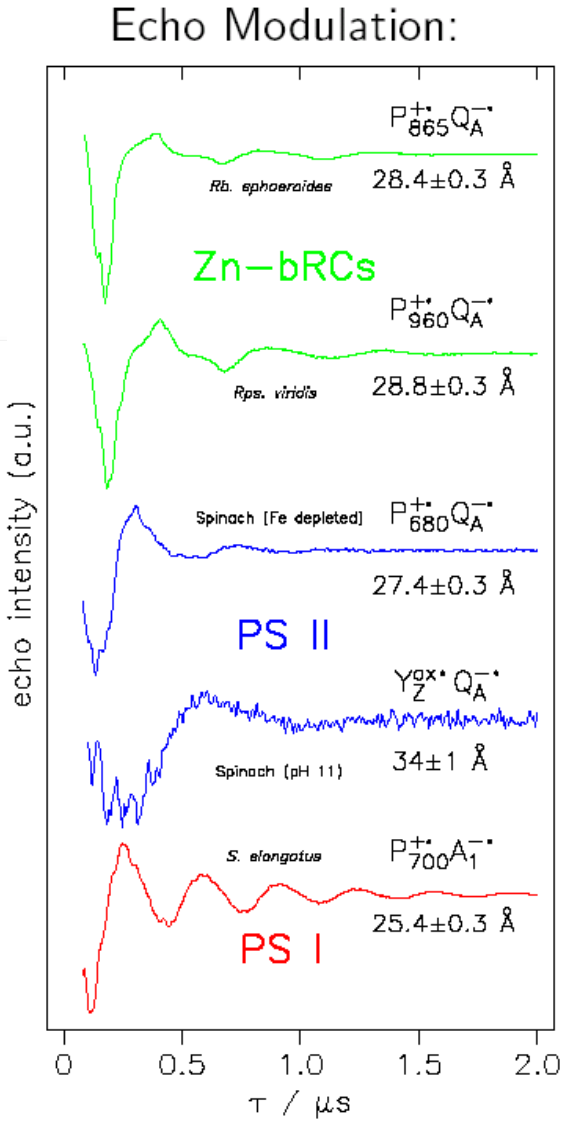

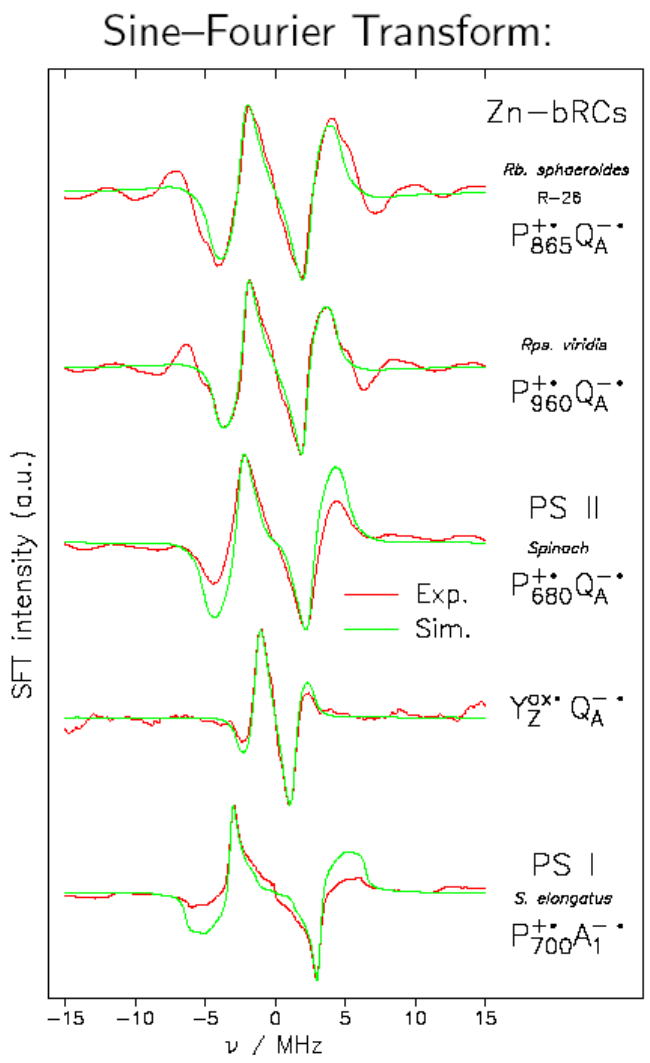

Dzuba S.A. and Hoff A.J. (2002) in: Berliner L.J., Eaton G.R., Eaton S.S. (eds) Distance Measurements in Biological Systems by EPR. Biological Magnetic Resonance 2002, vol 19. Springer, Boston, MA

Metal Cofactors and Metal Clusters

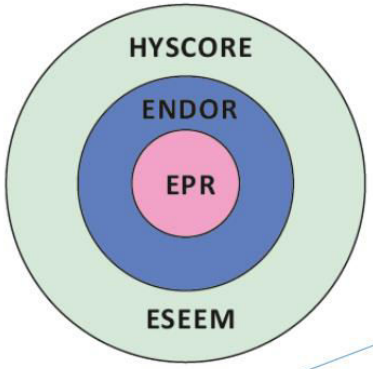

Remote nuclei:
ENDOR, ESEEM, HYSCORE
hyperfine coupling and
nuclear quadrupolar tensors

Directly coordinated nuclei:
ENDOR
hyperfine coupling and
nuclear quadrupolar tensors

Transition metal ions:
EPR, ENDOR, ELDOR-detected NMR
g tensor ,
metal hyperfine coupling
and zero field splitting tensors

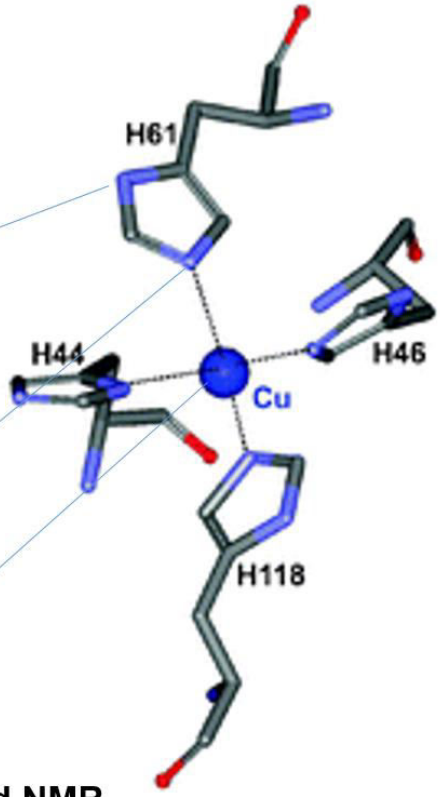

Type 2 Copper site

Water splitting
catalyst of Photosystem II:
tetramanganese-calcium
cluster

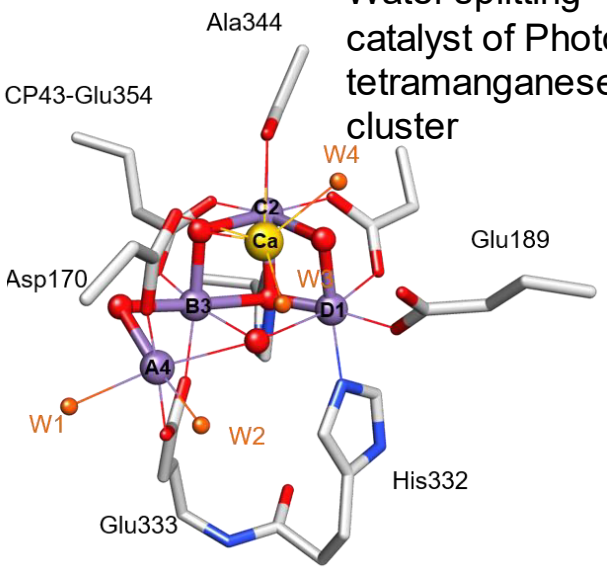

Umena et al. Nature 2011, 473, 55

Ni–Fe active
center
of *Desulfovibrio*
Hydrogenase

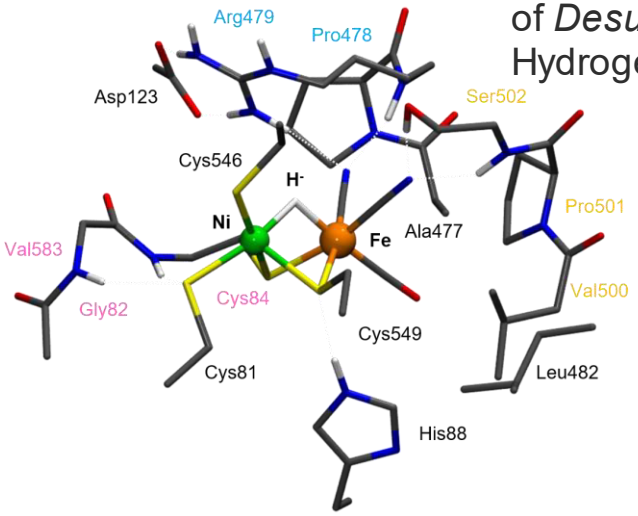

Higuchi et al. Structure1997, 5, 1971

EPR Spectra of the S states of the Water Splitting Catalyst

Strong spin coupling of Mn electrons leading to an effective spin state of the whole Mn_4O_5Ca cluster

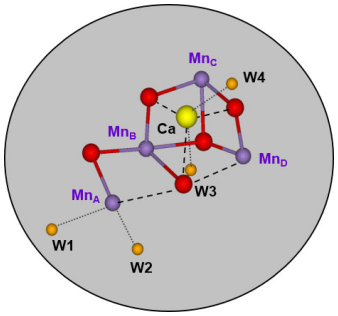

Mn(II) S=5/2
Mn(III) S=4/2
Mn(IV) S=3/2
Mn(V) S=2/2, 0
Ca(II) S=0

Nuclear spins (^1H, ^{55}Mn)
→ hyperfine structure

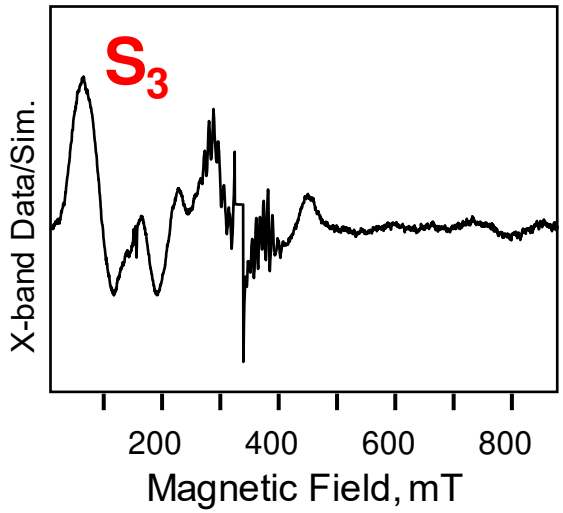

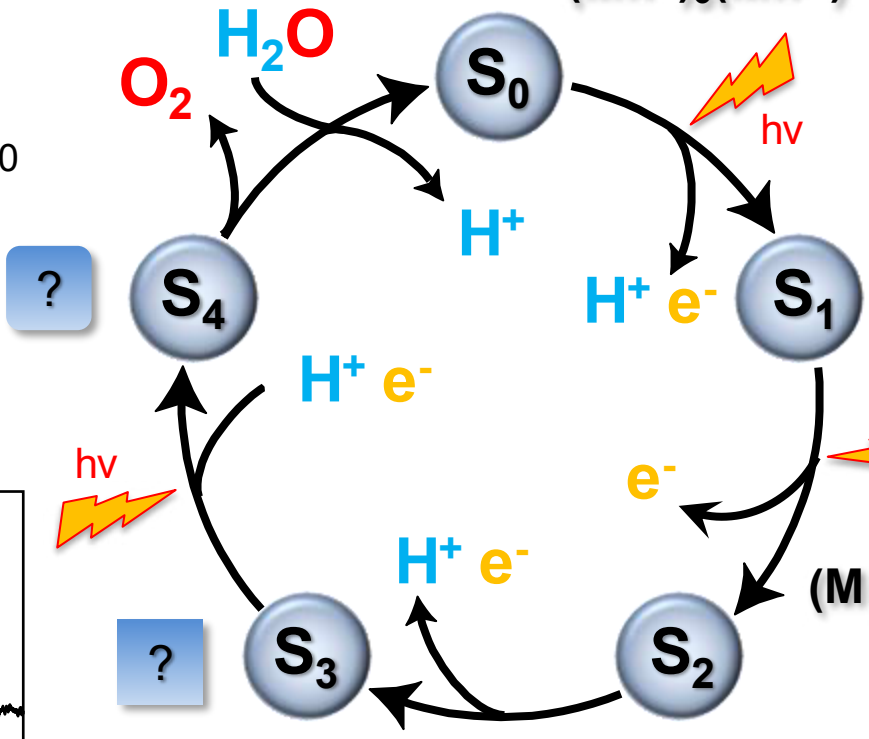

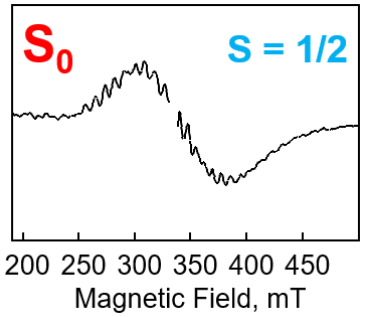

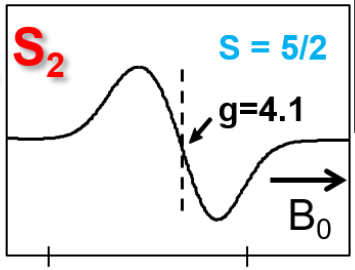

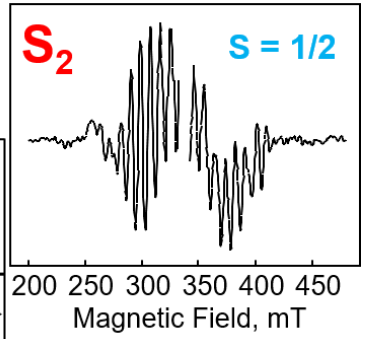

Cox et al., Science 2014, 345,804

Spectroscopic Characterization of the S_3 State of the Mn_4O_5Ca Cluster

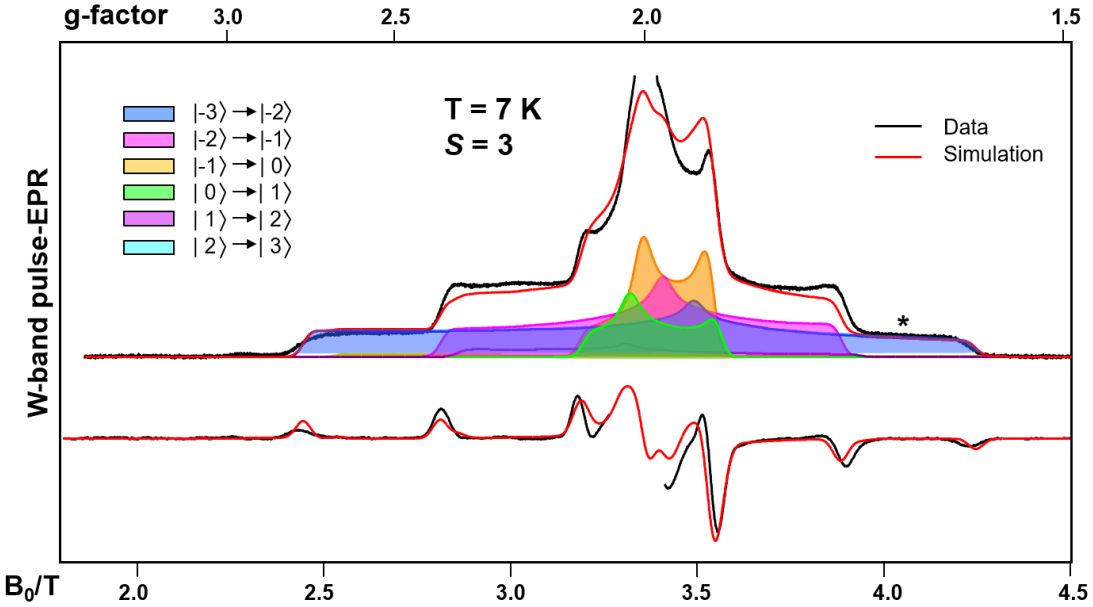

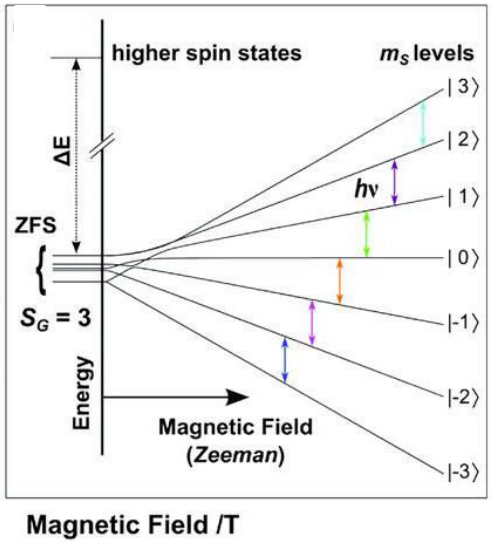

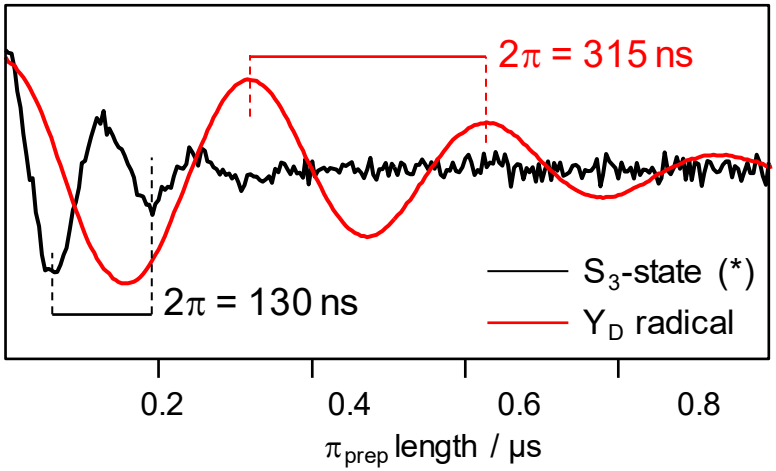

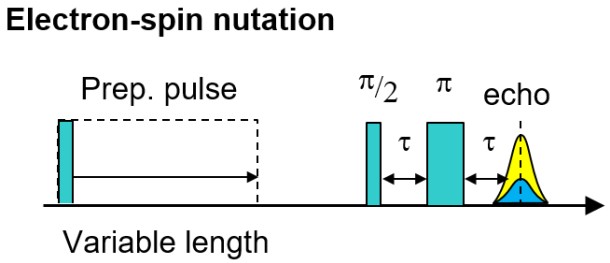

S=3 spin state

Ferromagnetic couplings: the S_3 state structure contains a 'complete' cubane unit, without open coordinate sites and all Mn(IV) ions.

Cox et al., Science 2014, 345,804

ELDOR-detected NMR of the S_3 State of the Mn_4O_5Ca Cluster

S=3 ^{55}Mn I=5/2

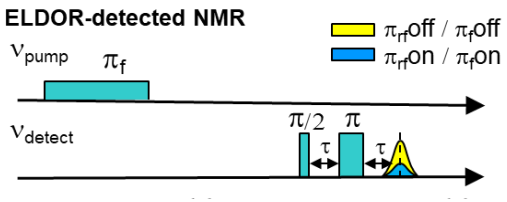

Two classes of ^{55}Mn hfcs: strongly and weakly coupled. Two of the Mn ions must have a small contribution to the ground spin state, whereas the other two ions have a large contribution.

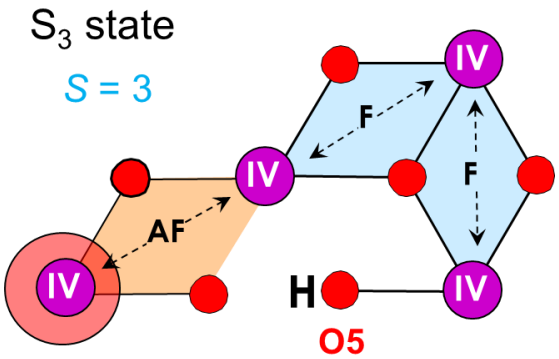

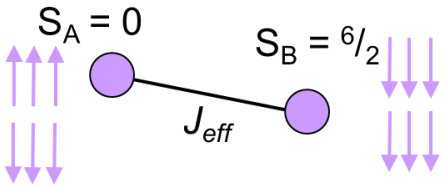

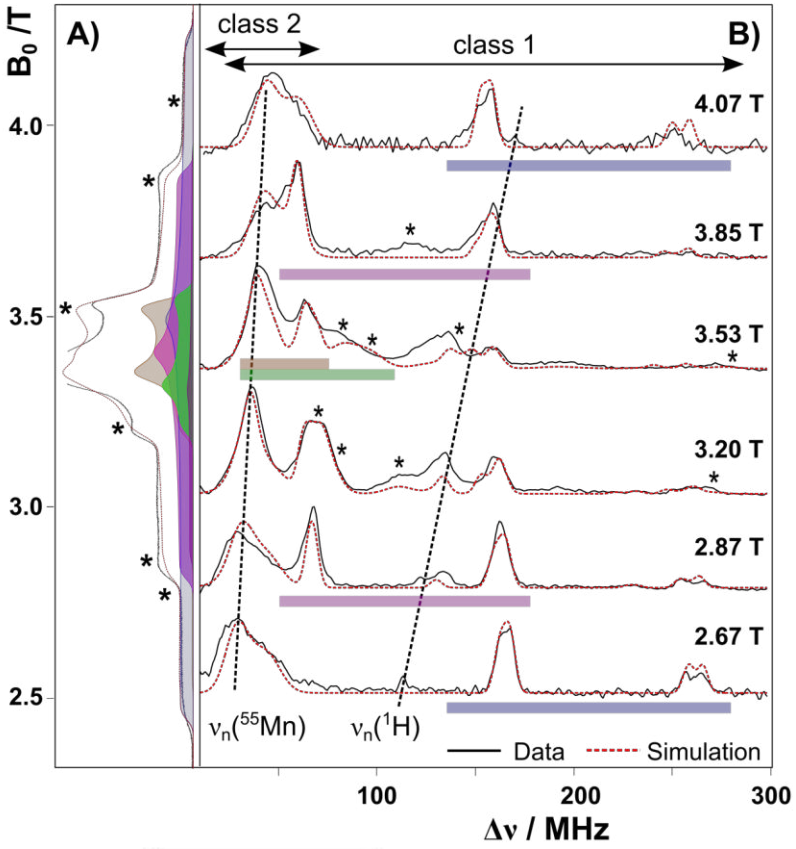

A dimer of dimers coupling topology: an open cubane including a substrate water in the form of hydroxyl group.

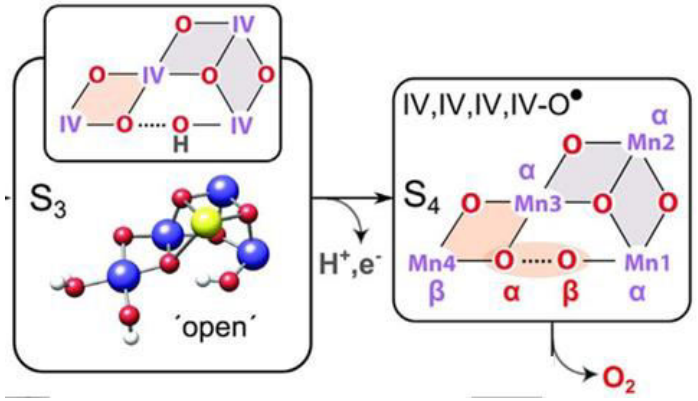

Cox et al., Science 2014, 345,804

Spectroscopic Characterization of the NiFe Hydrogenases

$H_2 \leftrightarrows H^- + H^+ \leftrightarrows 2H^+ + 2e^-$

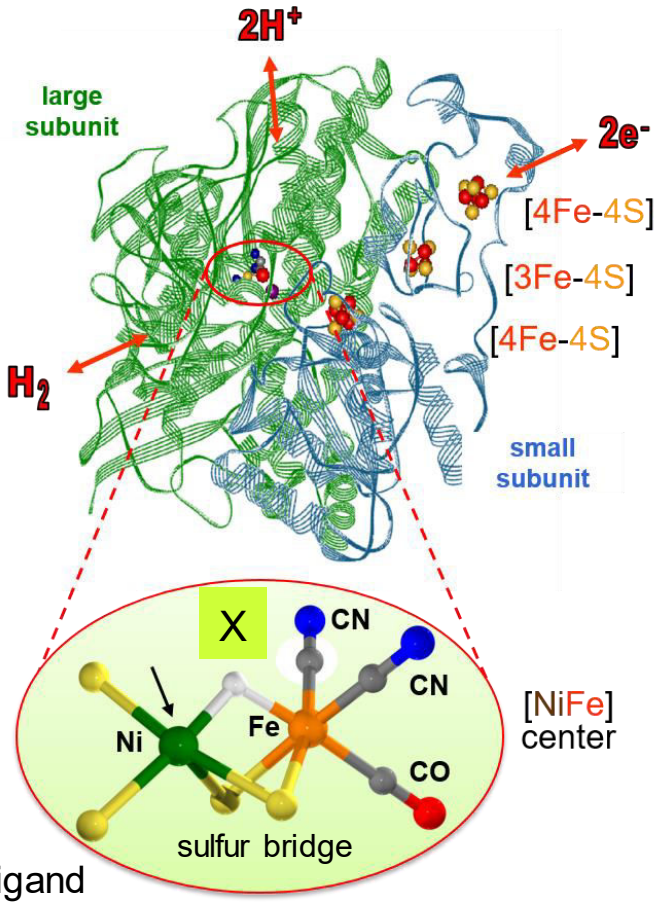

bridging ligand

X= HOO^-? (A), HO^- (B), H^- (C), empty (L)

[NiFe] Hydrogenase from D. vulgaris MF

^{61}Ni I=3/2 S=1/2

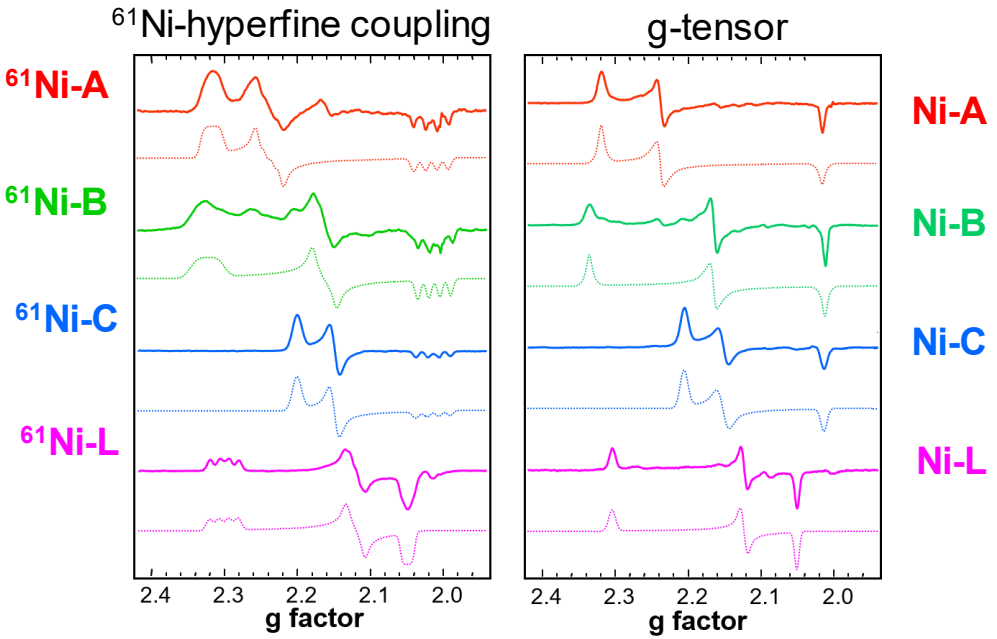

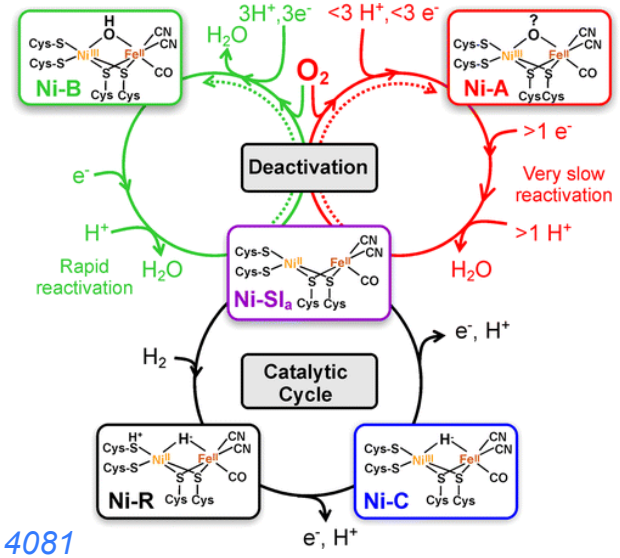

Higuchi et al. Structure1997, 5, 1971 *Lubitz et al. Chem. Rev. 2014, 114, 4081*

Evidence for a Hydride Bridge via ^{2}H ENDOR and ^{2}H HYSCORE

Hydride Bridge ?

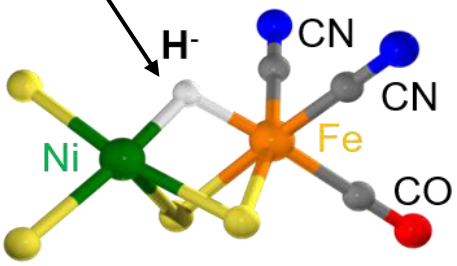

Structure of the active intermediate **Ni-C** state

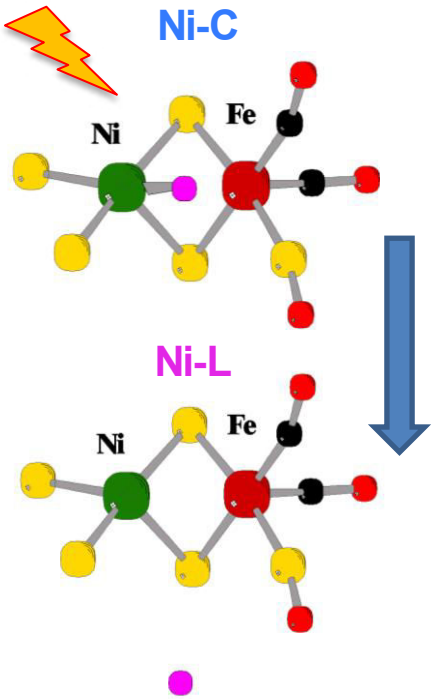

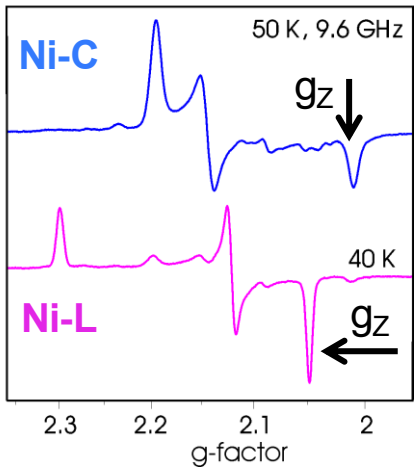

Illumination with white light: conversion of **Ni-C** in the **Ni-L** state

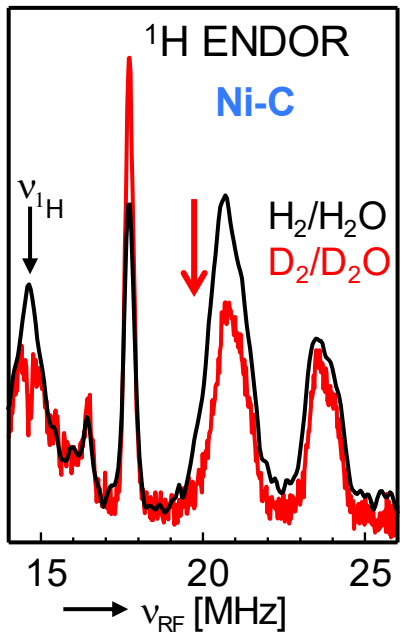

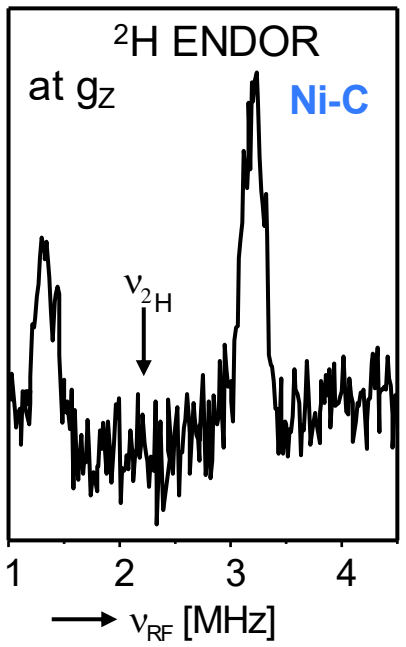

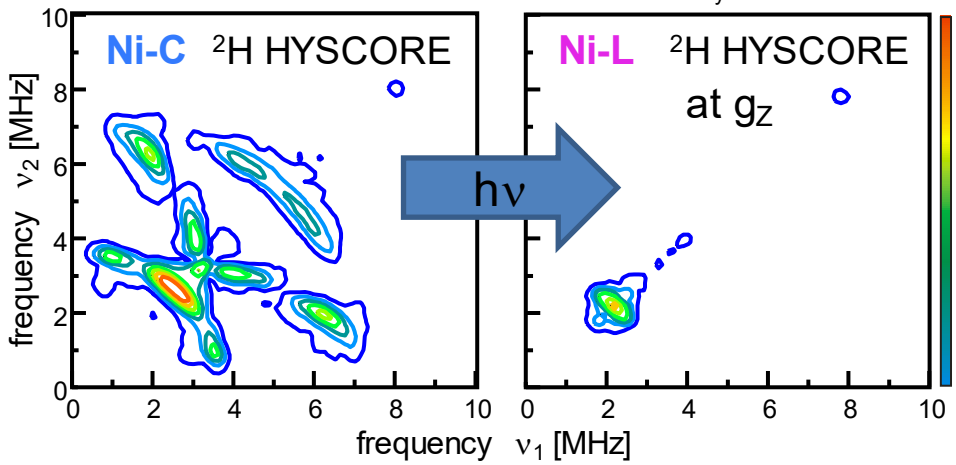

H/D Exchanged NiFe-Hydrogenase RH of *R. eutropha*

Brecht et al. JACS 2003, 125, 13075

Most common nitroxide spin labels

Highly reactive methanethiosulfonate group is specific toward cysteines

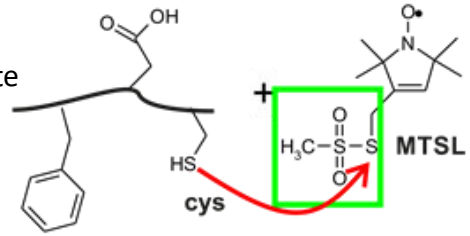

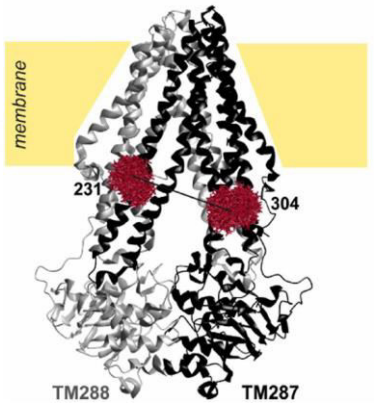

Bordignon et al. BBA 2018, 1860, 241

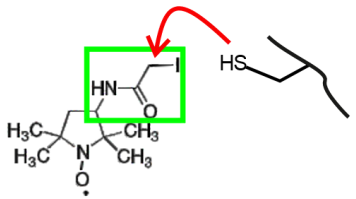

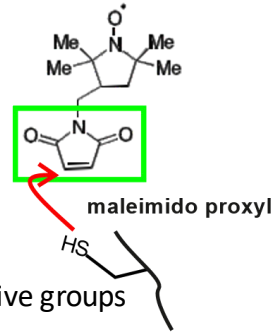

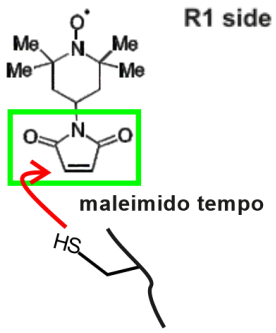

iodoacetamide or maleimide reactive groups

Nitroxides and unnatural amino acids

Bifunctional, conformationally restrained nitroxides

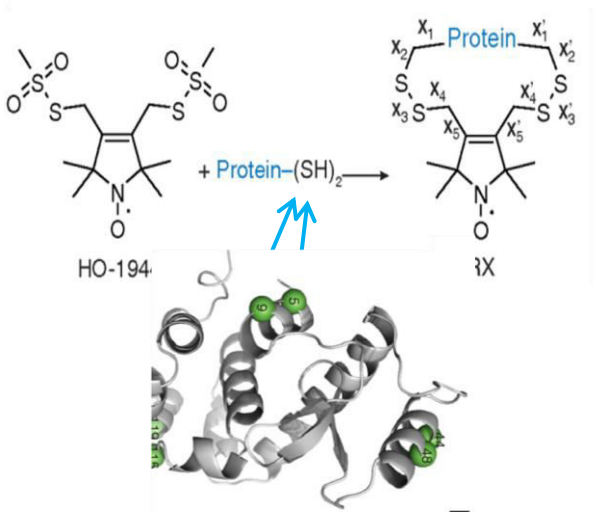

Fleissner et al. PNAS 2011, 108, 16241

genetically encoded unnatural amino acid

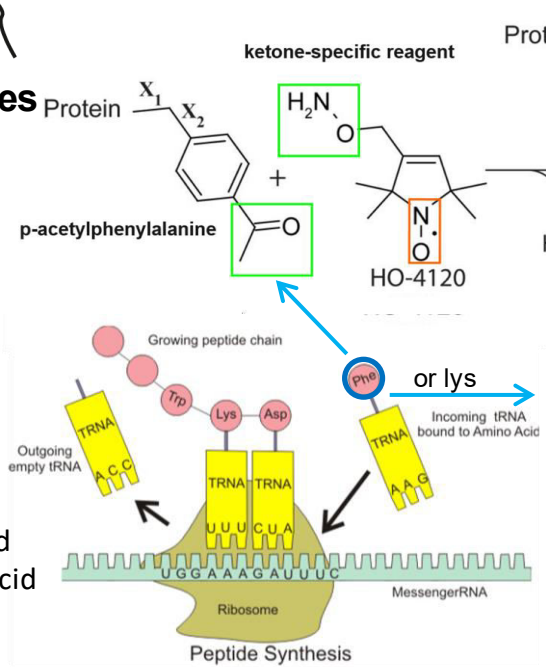

Fleissner et al. PNAS 2009, 106, 21637

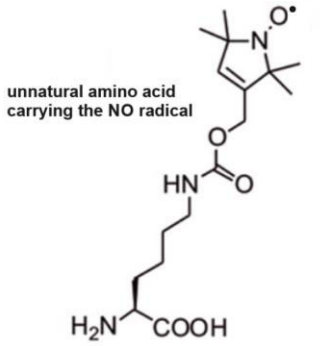

Schmidt et al. JACS 2014, 136, 1238

Orthogonal Labeling Approach

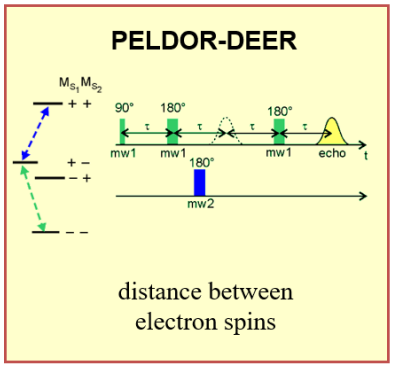

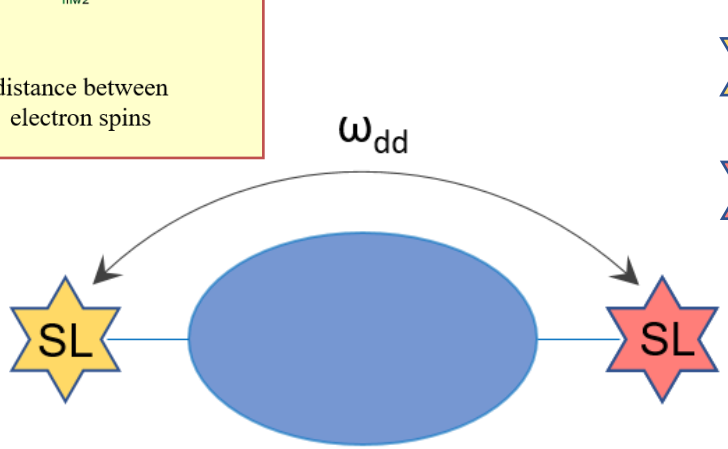

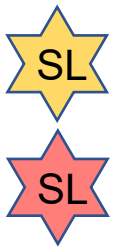

=

- NO˙
- Trytil

Radical spin labels

- Gd(III)
- Mn(II)

Metal-based tags

- Cu(II)
- Fe-S cluster
- Fe(III)

Spin label

Endogenous probes

ORTHOGONAL LABELING

Gd-based labels: most common spectroscopically orthogonal labels to nitroxide

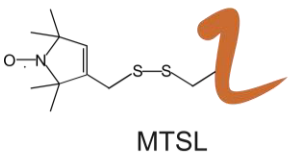

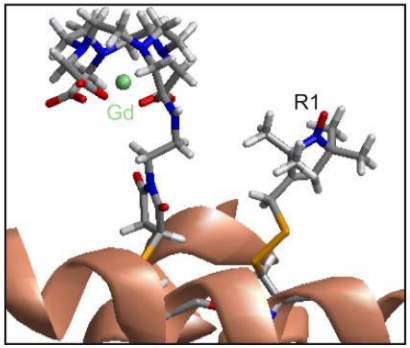

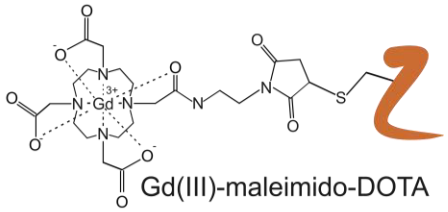

Goldfarb et al. Phys.Chem.Chem.Phys., 2014, 16,9685

ABC transporters harness the energy of ATP to pump substrates across membranes

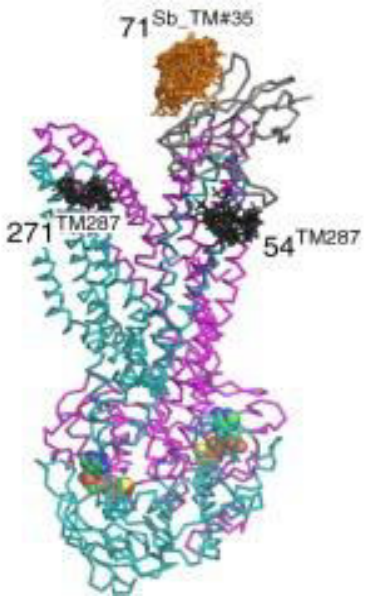

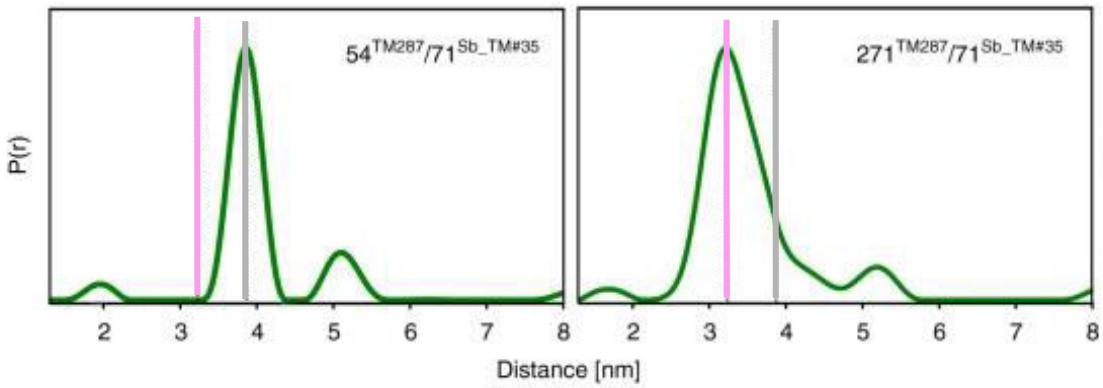

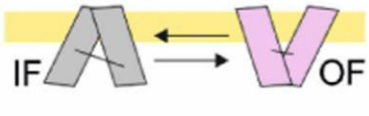

This ABC transporter switches from the **inward-facing state** (distance between spin labels at positions 231 and 304 3.5 nm) to the **outward-facing state** (distance between labels decreases to 2.5 nm)

ABC transporter TM287/288

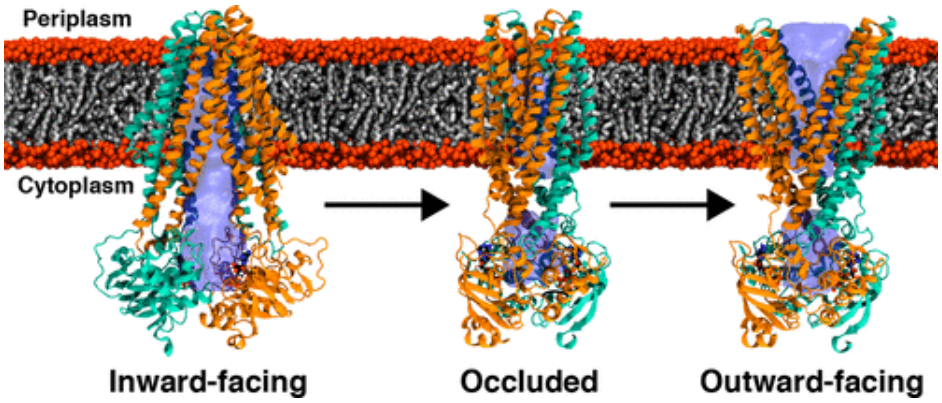

In response to ATP binding, the protein undergoes spontaneous **conformational transition** from **the inward-facing state** via an **occluded intermediate** to an **outward-facing state.**

Hutter et al. Nature Comm. 2019, 10, 2260

Orientation-Selective DEER Spectroscopy

Orthogonal labelling and endogenous probe: X-band DEER on $[Fe_2S_2]^{+\bullet}$ - $NO^{\bullet}$

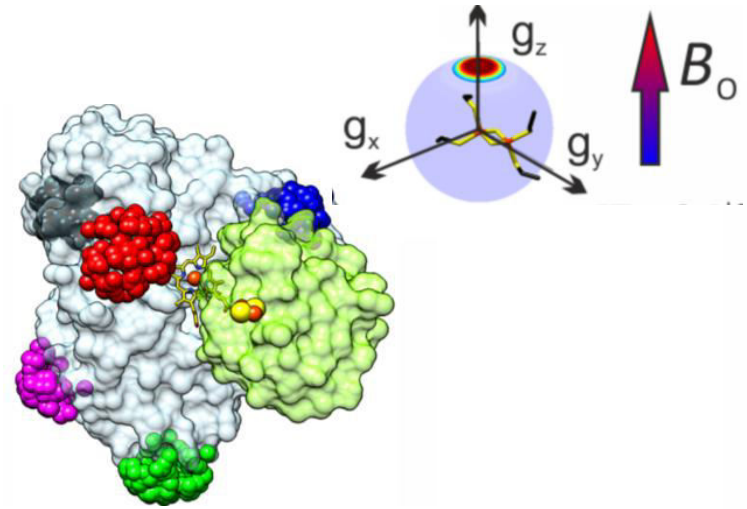

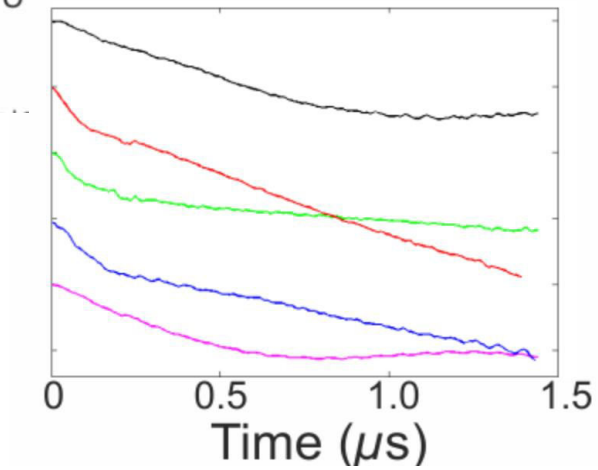

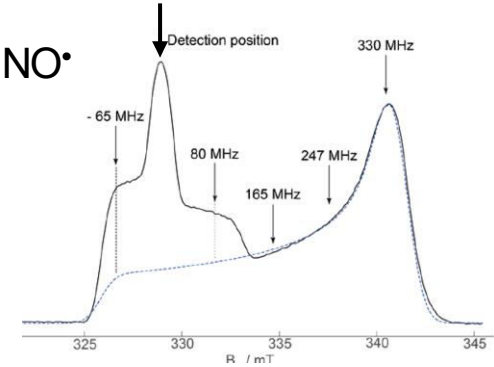

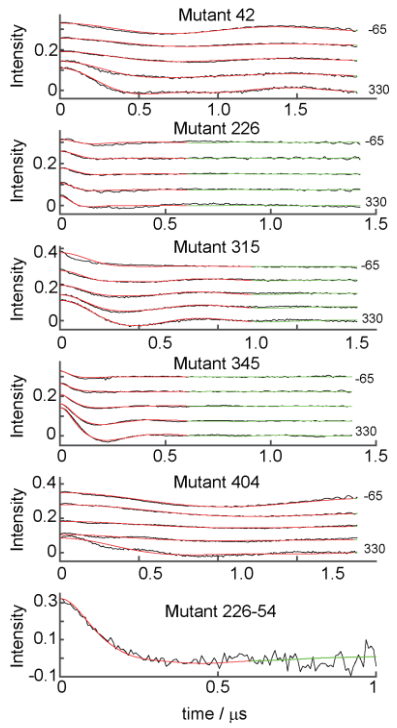

Structural model for the **cytochrome P450 monooxygenases** (grey) - **ferredoxin** (light green) **complex** as deduced from orientation-selective DEER spectroscopy.

Cartoon representation of the best six DEER-docked structures of the protein complex

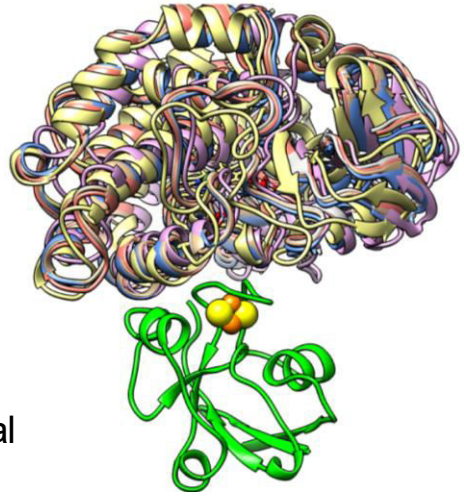

The structural model was refined minimizing the difference between the simulated and experimental DEER traces

For each mutant X-band DEER at different pump to detection frequency offsets

Bowen et al. J. Am. Chem. Soc. 2018, 140, 2514−2527

Light-Induced DEER: Triplet state Probe

Porphyrin-based spectroscopic ruler

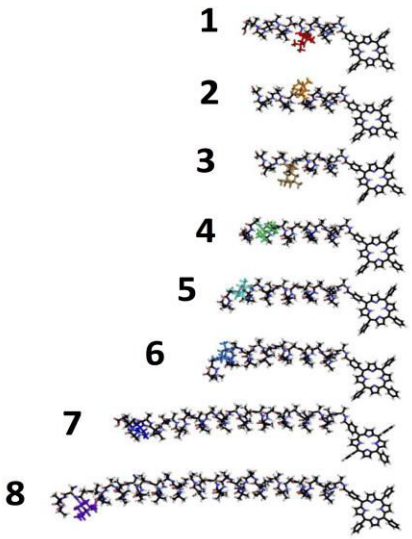

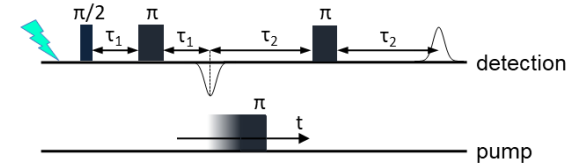

Light-induced DEER

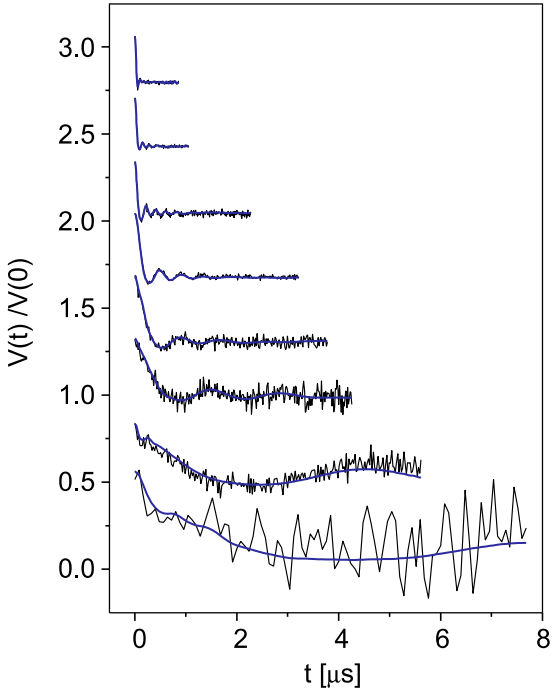

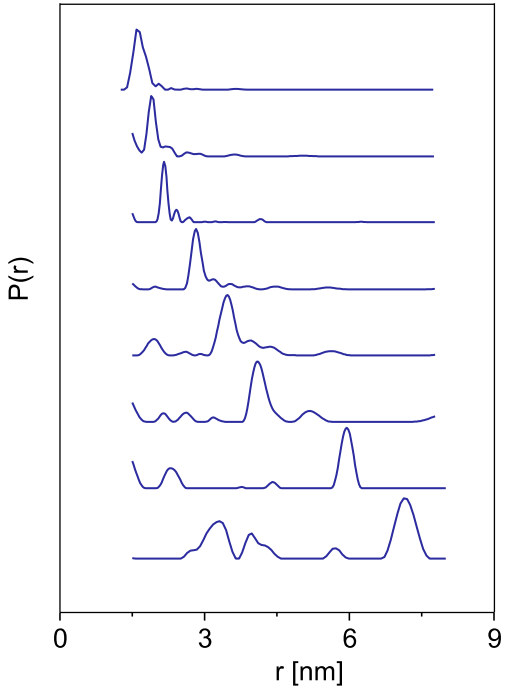

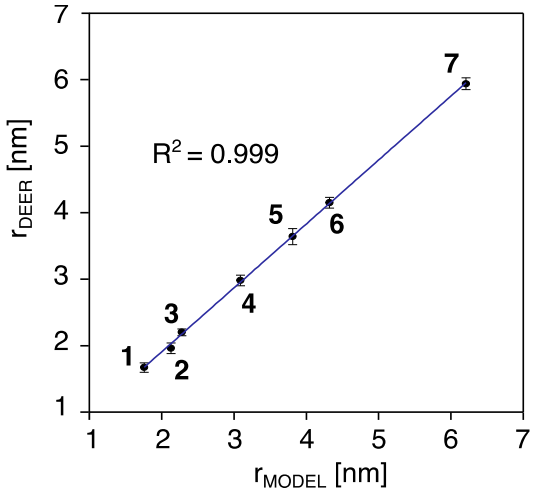

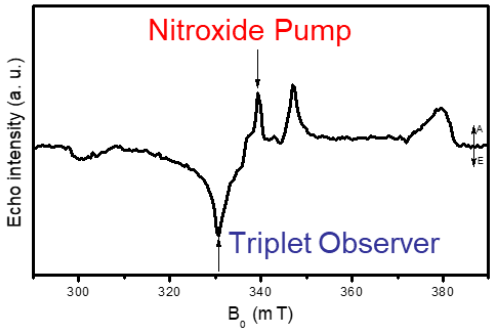

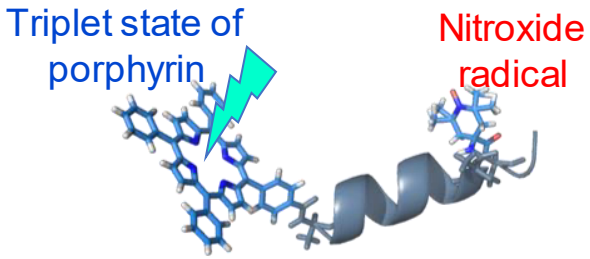

Di Valentin, Chem. Eur. J. 2016, 22,17204

Light-Induced DEER in Heme Proteins

Substitution of the heme with Zn(II) Protoporphyrin IX

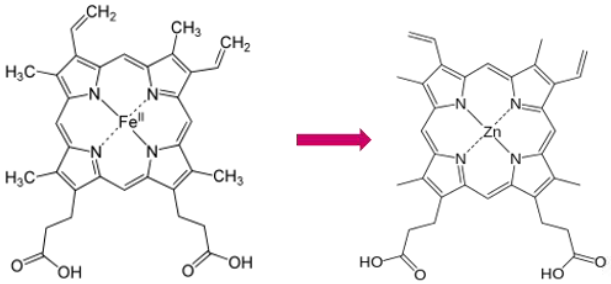

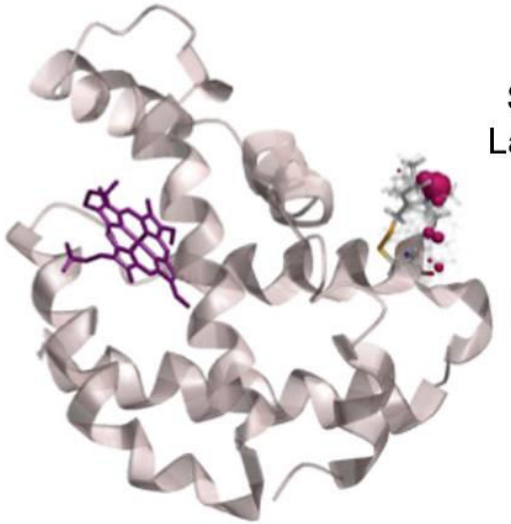

Site-Directed Spin-Labeling with MTSSL

HUMAN NEUROGLOBIN

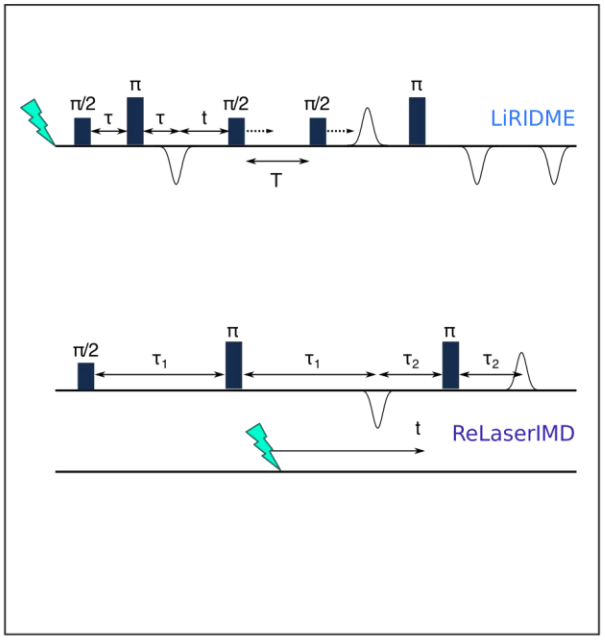

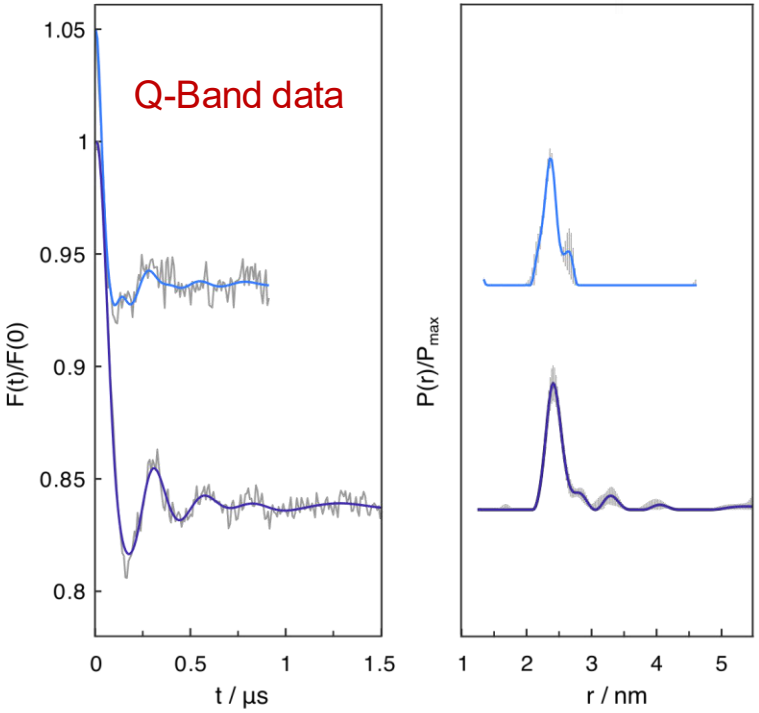

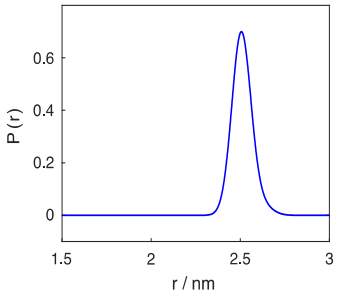

Distance distribution predicted by MMM

*Di Valentin et al. ChemPhysChem, **2019**, 20, 931*

Conclusions

Radicals

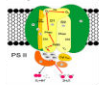

Identification of radical species, light-induced or chemically oxidized in Photosystem II, by CW-EPR and High-Field EPR

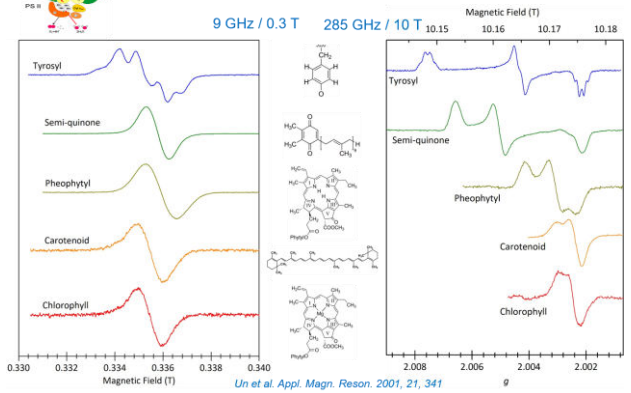

Un et al. Appl. Magn. Reson. 2001, 21, 341

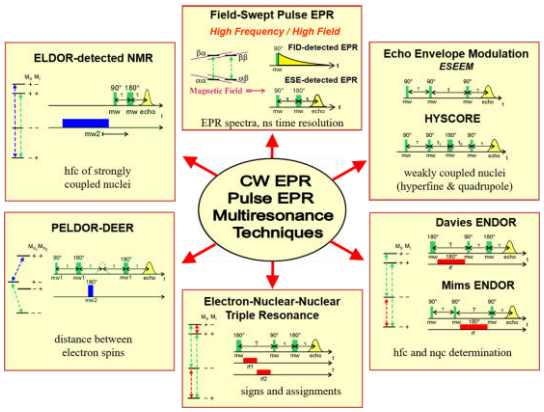

Spin Labels

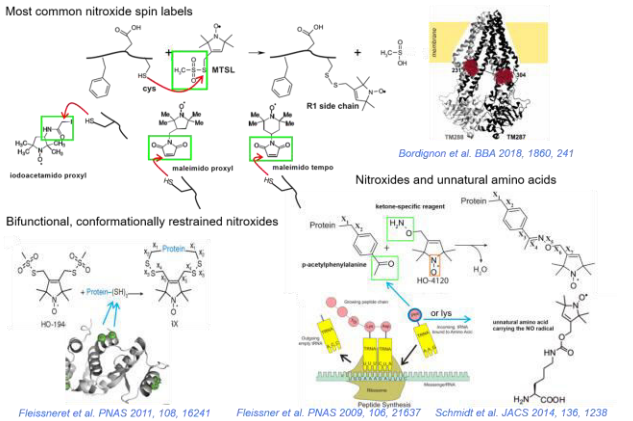

Metal Cofactors

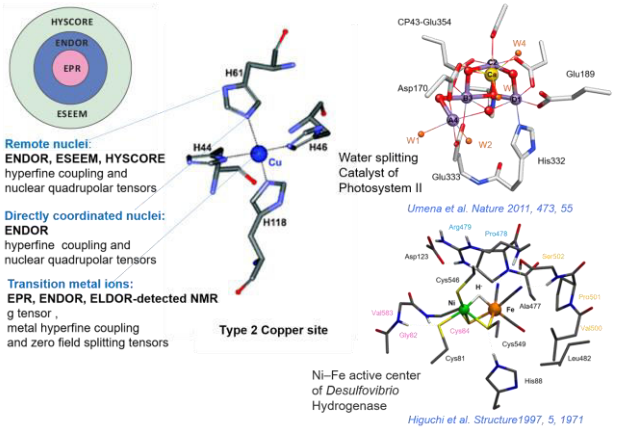

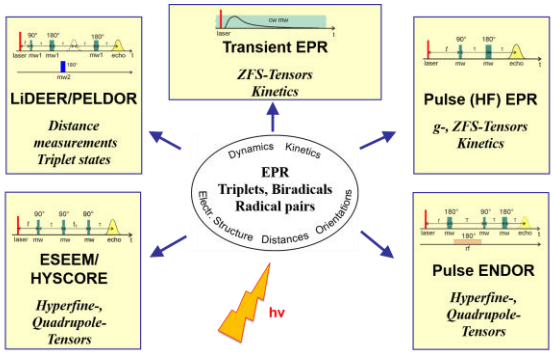

Triplet States Radical Pairs

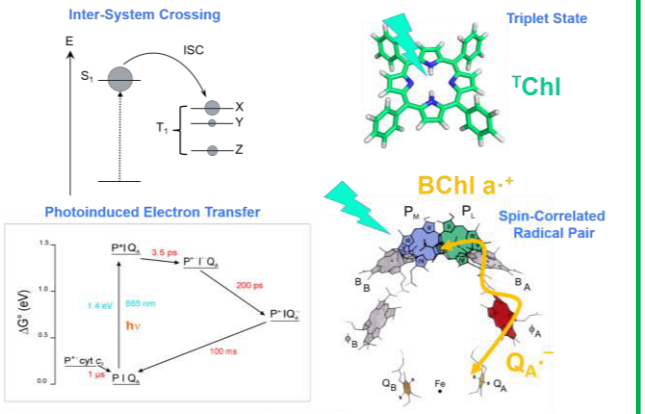

EPR has a wide range of **biological applications**, even for samples that are not paramagnetic to begin with. **Advanced EPR techniques** in combination with **state-of-art computational methods** provide detailed information on the structure and the electronic properties of biomolecules.